UCRL-53076
Distribution Category UC-70

In Situ Geomechanics Climax Granite, Nevada Test Site

F. E. Heuze*
W. C. Patrick*
R. V. De la Cruz†
C. F. Voss†

April 1981

*Earth Sciences Division, Lawrence Livermore National Laboratory
†Department of Mining Engineering, University of Wisconsin, Madison

LAWRENCE LIVERMORE LABORATORY
University of California • Livermore, California • 94550

FOREWORD

This project was supported under the Department of Energy's National Waste Terminal Storage Program and was administered through the Nevada Operations Office as part of the Spent Fuel Test in Climax Stock granite (SFT-C) at the Nevada Test Site (NTS).

Dr. F. E. Heuze directed the project and wrote this report. He was assisted in the field by Dr. W. C. Patrick. Professor R. V. De la Cruz and his assistant, Mr. C. F. Voss--both from the Department of Mining Engineering at the University of Wisconsin, Madison--participated as consultants and performed some of the field tests.

Mr. D. Wilder contributed to the definition of the geology at SFT-C and provided rock quality designation (RQD) values. Mr. J. Norman and Dr. N. Burkhard aided in the analysis of the shear wave records. Ms. D. Olson typed the manuscript. Ms. Carol Gerich was the report's technical editor. Their assistance is gratefully acknowledged.

CONTENTS

IN SITU GEOMECHANICS
CLIMAX GRANITE, NEVADA TEST SITE

ABSTRACT

The in situ modulus of the Climax granite in the Spent Fuel Test (SFT-C) area of the Nevada Test Site was estimated using six different approaches. Our best estimate of field modulus as E_f = 26 GPa was obtained from a comparison of the various approaches. A best estimate of laboratory modulus acquired by comparing three different sources was E_ℓ = 70 GPa. Therefore, the modulus reduction factor for the Climax granite appears to be E_f / E_ℓ = 0.37. In turn, our estimate of in situ rock-mass deformability was used to back-calculate in situ values for the normal stiffness of the granite joints.

Our analysis of former stress measurements by the U.S. Geological Survey (USGS) shows that the horizontal stresses in the vicinity of SFT-C vary greatly with azimuth. An unexplained feature of the stresses at SFT-C is the fact that the vertical stress appears to be only 65 to 75% of the calculated lithostatic burden. From the three-dimensional stress ellipsoid at mid-length in the tunnels, assuming a plane strain condition, we were able to estimate an in situ Poisson's ratio of the rock mass as ν = 0.245. Two other techniques were applied in an attempt to measure the stresses around the SFT-C heater and canister drifts: the undercoring method and the borehole jack fracturing approach. The former technique appears to have given reasonable estimates of tangential stresses in the roof of the heater drift, while the latter appears to give low results for stresses in the pillars.

Specific recommendations are made for future tests to further characterize the mechanical properties of the Climax granite and the in situ stresses at SFT-C.

1. INTRODUCTION

1.1 SPENT FUEL TEST (SFT-C) MINE-BY EXPERIMENT

1.1.1 Mine-by at SFT-C

Lawrence Livermore National Laboratory (LLNL) is conducting a generic test of retrievable geologic storage of nuclear spent fuel assemblies in an underground chamber at the Nevada Test Site (NTS), Nye County, Nevada.[1,2] This generic test is located 420 m below the surface in Climax granite. Eleven canisters of spent fuel, approximately 2.5 years out of reactor core (about 1.6 kW/canister thermal output), are now emplaced in a storage drift along with six electrical simulator canisters. Two adjacent drifts contain electrical heaters, which will be operated to simulate the thermal field of a large repository.

The three drifts are shown in Fig. 1. Their excavation was performed in three steps: the two heater drifts were excavated first, then the top heading of the canister drift was mined, and finally, the bench was removed. Prior to the mine-by of the center (canister) drift, deformation and stress gages were emplaced near two cross sections, labeled stations 2+87 and 3+45 (Fig. 2.).

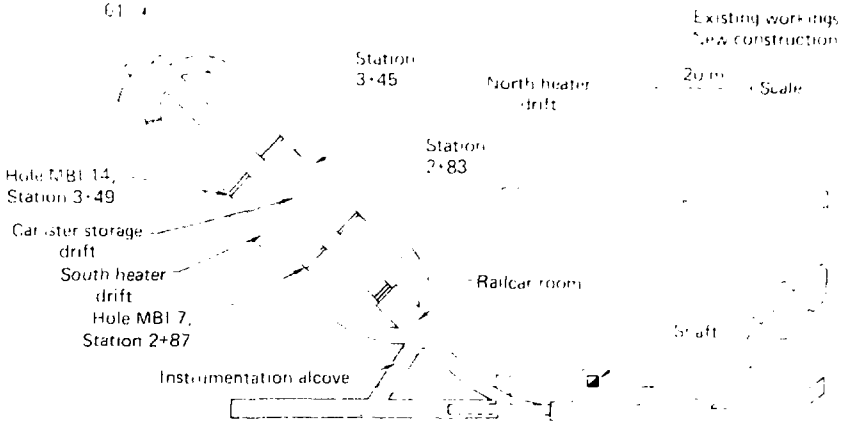

FIG. 1. Spent Fuel Test layout in Climax granite, NTS.

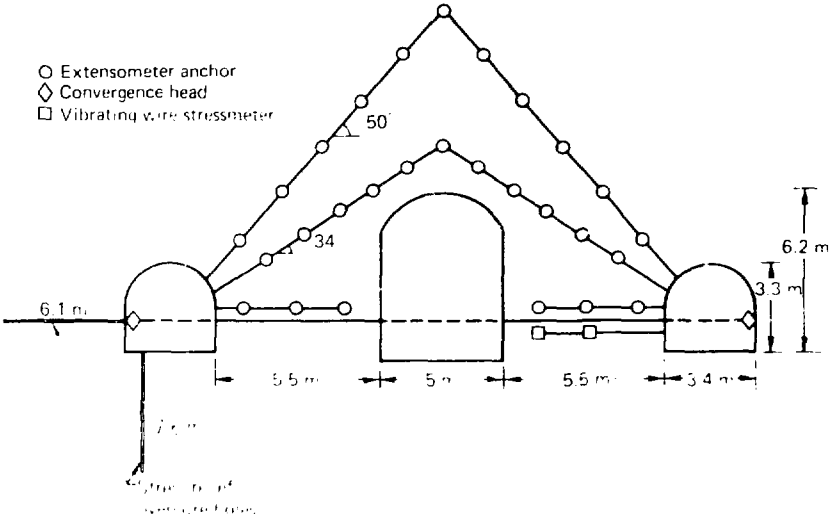

FIG. 2. Schematic cross section of Spent Fuel Test, showing relative location of mine-by instruments (reproduced with permission from Ramspott and Ballou[2]).

1.1.2 *Modeling of the Mine-by*

Two calculations related to the mine-by were reported previously.[1,3] In neither case did the numerical models explicitly include the geological discontinuities such as joints and shears. The rock-mass modulus was chosen from handbook values, since no field tests had been performed to estimate it. In the first model[1] the ratio of horizontal to vertical stresses varied between 0.8 and 1.0; in the second model[3] it ranged from 0.8 to 1.25. The highest value of 1.25 is close to that derived from the analysis of overcoring measurements conducted by the U.S. Geological Survey around the south heater drift. Neither model had the capability to represent dilatancy or strain-softening of the rock mass.

The stress changes and deformations calculated by LLNL[1] with the ADINA code are summarized in Table 1 and Fig. 3. Stresses and deformations calculated by Terra Tek, Inc.[3] with the DIG and TWODY codes were quite

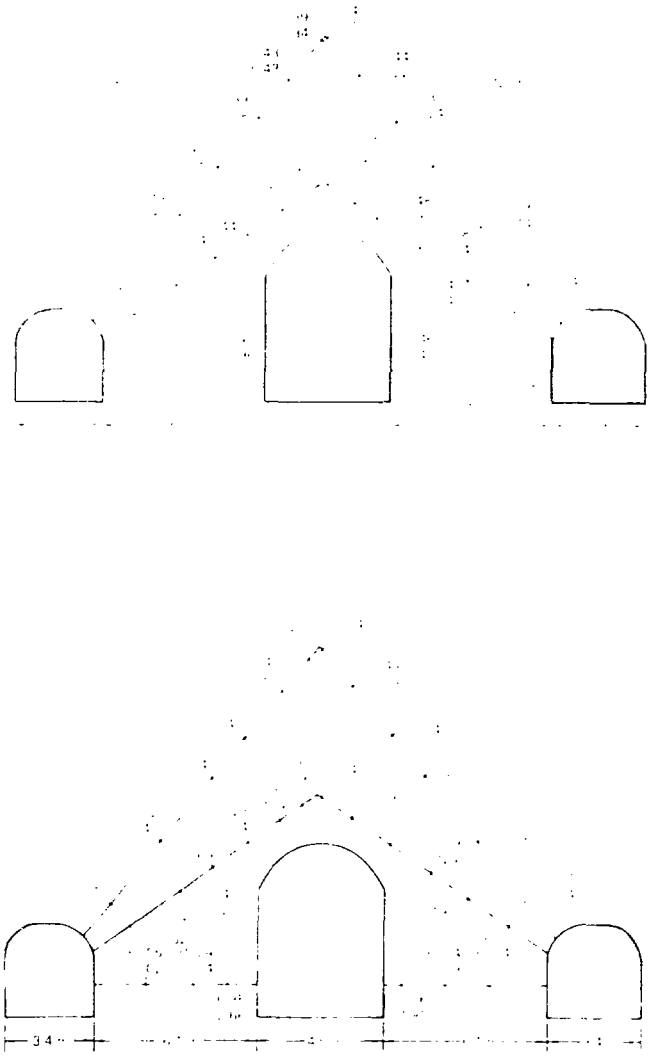

FIG. 3. Comparison of measured and (predicted) displacements during mine-by at SFT-C (reprinted with permission from Ramspott[1]).

TABLE 1. Comparison of measured and previously calculated vertical stress changes, as a result of the mine-by (data from Ramspott[1]).

Stress-meter No.	Station (Fig. 1)	Dist. from canister drift (m)	VSM[a] reading (MPa)	Calculated[b] stress change (MPa)
VSM-1	2+80	1.0	-9.7	+5.1
VSM-2	2+80	3.0	-1.3	+2.3
VSM-3	3+02	1.0	-7.0	+5.1

[a]Vibrating wire stressmeter (VSM) calculations assumed a rock modulus of 61 GPa. Minus sign indicates a decrease in compression.

[b]Rock modulus assumed at 61 GPa. Horizontal-to-vertical stress ratio taken as 0.8.

similar. This was to be expected, considering the similarity of the input. The results of modeling can be summarized as:

- The models did not show a reduction in vertical stresses in the pillars during mine-by of the canister drift, as reported from the field.[1,3]
- The models did not show a horizontal contraction of the pillars during mine-by, as reported from the field.[1,3]
- The relative movements of anchors for the extensometers at 34° to the horizontal were several times larger than predicted by the models at stations 3+45 and 2+83.
- The relative movements of anchors from the extensometers at 50° to the horizontal were in slightly better agreement with the predicted values at both stations.

In general, observations and calculations came closer to each other as one moved away from the drifts.

1.1.3 Discussion

The decrease in vertical stress at vibrating stressmeters VSM-1 and VSM-3 can be explained from the softening of the rock in the skin of the pillars, as

a result of blasting and stress relief that open up fractures. Also, the decrease at VSM-2 in the core of the pillar is not unreasonable; our new analysis of the mine-by[4] indicates that localized pillar unloading can take place, depending upon the geometry of the joints and shears, even when the average vertical pillar stress increases.

The reported horizontal contraction of the pillars, however, is more puzzling. In a previous report[3] the horizontal shrinkage of the pillars was explained by saying that stress arching took place over the caverns; however, the arching hypothesis was not substantiated. Arching would mean that the pillars unloaded through some load redistribution on the abutments, but the lack of stress gages in the abutments prevents confirmation of this. Whatever truly happened, the horizontal shortening of the pillars could only take place through one of three modes (Fig. 4):

- Unloading before peak.
- Unloading postpeak.
- Offloading in a so-called Class II behavior, only because Class I behavior gives a strain increase.

There is no published evidence that the Class II offloading observed with servo-controlled machines in laboratory compressive tests can exist in the field, where vertical loading is passive due to the overlying rock.

As for the unloading assumption, a simple calculation shows the strange conclusion to which it leads. The average pillar shrinkage at four locations (Fig. 3) is at least equal to

$$(1.96 + 1.42 + 2.66 + 1.80)/4 = 1.86 \text{ mm} .$$

For pillars with an average width of 5.5 m, this corresponds to a horizontal unloading strain recovery:

$$\Delta\varepsilon_{hor} = 1.86 \cdot 10^{-3} / 5.5 .$$

With a Poisson's ratio $\nu = 0.246$, this implies a vertical strain recovery:

$$\Delta\varepsilon_{vert} = \Delta\varepsilon_{hor} / 0.246 = 1.4 \cdot 10^{-3} .$$

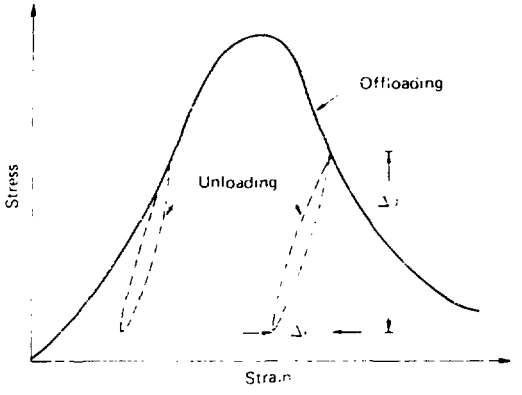

Class I strain softening

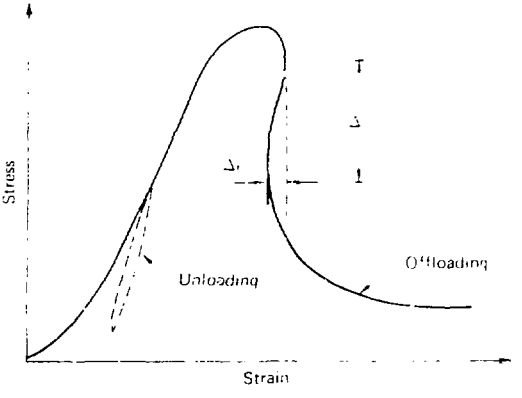

Class II strain softening

FIG. 4. Unloading vs offloading; stress-strain response.

From our best estimate of 26 GPa for the in situ modulus of the Climax granite, the above $\Delta\varepsilon_{vert}$ would require a vertical stress relief equal to

$$\Delta\sigma_{vert} = 26 \cdot 10^3 \cdot \Delta\varepsilon_{vert} = 36 \text{ MPa} .$$

Admittedly, the pillars start out in a triaxial state of stress, whereas the above calculation is uniaxial. Also, elastic behavior is assumed. Nevertheless, the 36-MPa figure is considerably in excess of the 1.3 MPa from VSM-2. In fact, it is considerably larger than the in situ vertical stress of 7.9 MPa reported at SPT-C. The pillars would end up in a state of large net tension, a very unique occurrence. Besides, our pillar stress measurements have indicated compression to exist.

In summary, it appears that the unique horizontal shrinkage of the pillars, reported earlier,[1,3] is neither consistent with model studies nor explained from stress-strain relations for the rock mass. On the other hand, there is no difficulty in providing reasonable explanations for the reported localized decreases in vertical pillar stress.[4]

To shed some light on the above riddle, a two-phase program was initiated in 1980. It consisted of a new modeling effort, using the JPLAXD finite element program,[5] and a field-related project to provide realistic input for the new models. The new model calculations, which are reported separately,[4] include:

- Representation of discrete geological discontinuities, such as major joints and shears observed around the tunnels.
- Strain-softening and dilatancy of joint and rock elements.
- Field-measured input of rock-mass modulus.
- Field-measured input of in situ stresses.
- Poisson's ratio derived from field stress measurements.
- Parametric variation of the horizontal-to-vertical stress ratio between 0.5 and 3.5.

1.2 Purpose and Scope of Project

This report describes the results of the field-related research conducted to obtain a more representative input for the JPLAXD models. The field work for this project consisted of:

- Detailed inspection of the three drifts, to identify the major geological discontinuities that should be represented discretely in the new models.
- Calculation of the rock quality designation (RQD) for cores obtained in NX-holes MBI-7 and MBI-14, which run horizontally through the pillars in the vicinity of stations 2+87 and 3+49 (Fig. 1).
- Rock-mass deformability tests in MBI-7 and MBI-14 with the NX-borehole jack and with a modified NX-jack, also used for stress measurements.
- Petite sismique tests across the two pillars in which the frequency of horizontally polarized shear waves was measured.
- Evaluation of the rock mass rating (RMR) and Q-rating for the Climax granite.
- Undercoring stress measurements at mid-length of each heater drift to obtain values of tangential roof, pillar, and rib stresses.
- Stress measurements in both pillars by borehole jack fracturing using holes MBI-7 and MBI-14.

1.2 Geologic Setting

The Climax stock at the Nevada Test Site is composed of quartz monzonite and granodiorite.[6] The Spent Fuel Test site is located in the quartz monzonite, which contains three sets of joints nearly perpendicular to each other[6]:

	Average strike	Average dip
Set 1	N32W	22NE
Set 2	N64W	Near vertical
Set 3	N35E	Near vertical

In addition, there are a number of shear zones intersecting the three drifts.[7]

For the new modeling of the mine-by, we selected two cross sections containing discrete discontinuities (Figs. 5 and 6). They constitute two-dimensional approximations in which only selected shears and master joints are included. Eventually, three-dimensional models with discrete joints should be used, since the strike of the major discontinuities at SFT-C is not parallel to the axis of the drifts; it is 10 to 30° off from the axis.

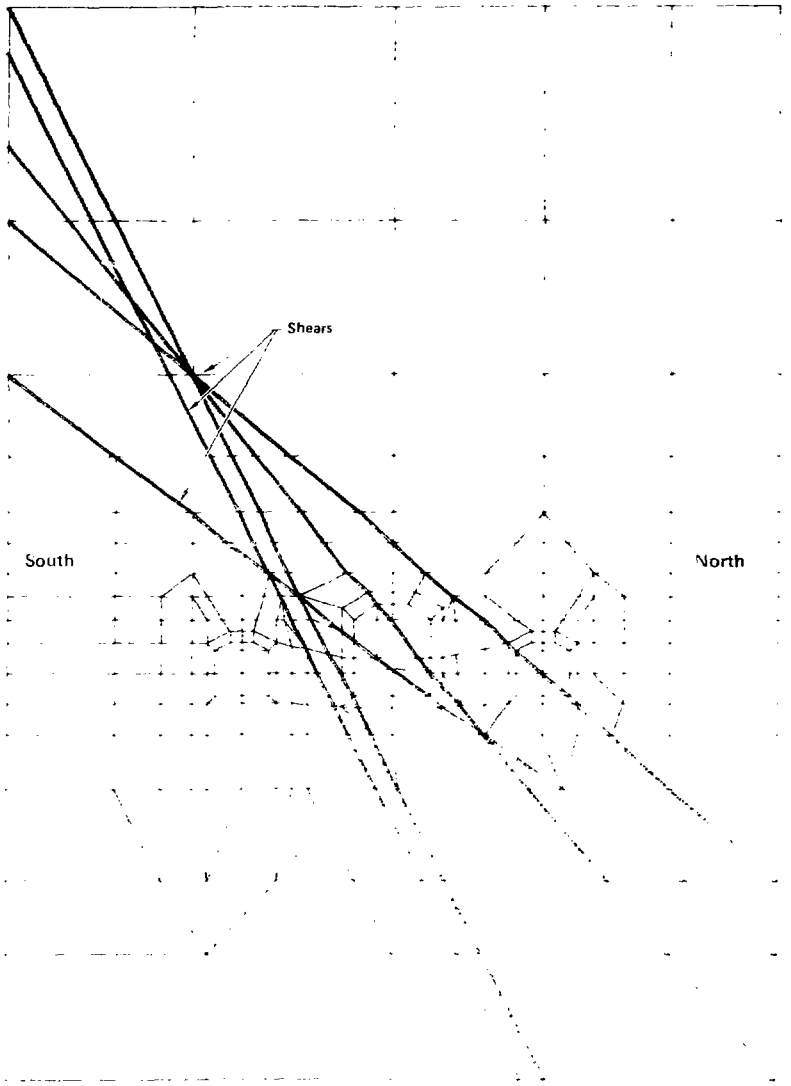

FIG. 5. Representative cross section for new mine-by analysis, station 2+83.

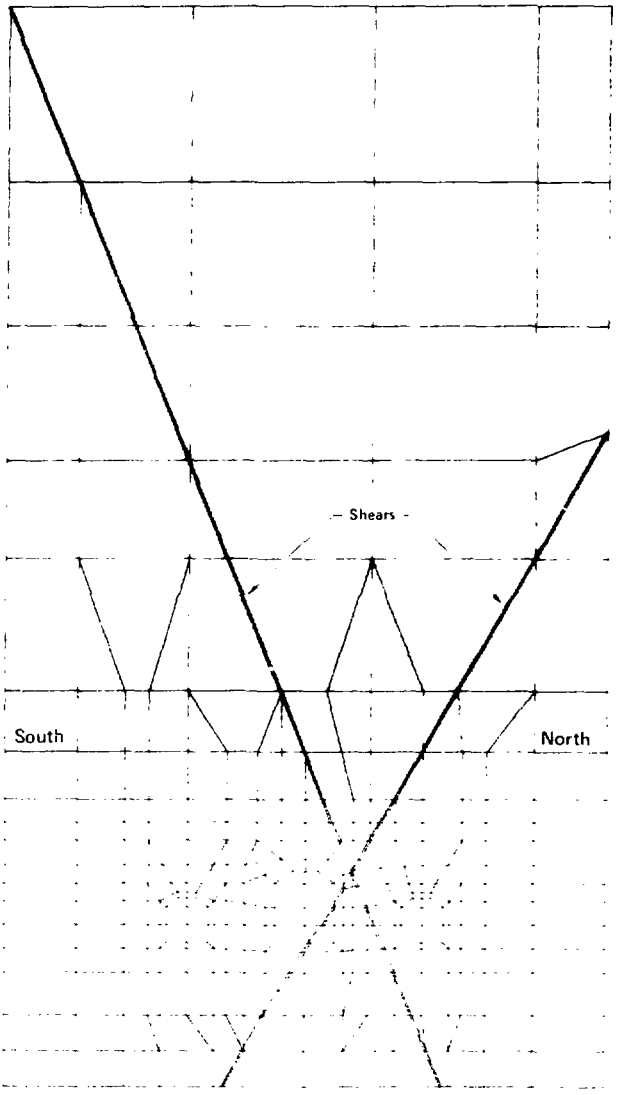

FIG. 6. Representative cross section for new mine-by analysis, station 3+45.

2. IN SITU DEFORMABILITY

2.1 NX-BOREHOLE JACK TESTS

2.1.1 The NX-Borehole Jack

The NX-borehole jack (Goodman Jack) used in this project was leased from Slope Indicator Co., Seattle, Wash. The instrument and the theory for data analysis have been discussed at length in the literature.[8-10]

2.1.2 NX-Jack Tests at SFT-C

For the purpose of measuring the deformability of the Climax granite in place, we took advantage of the availability of two NX-holes that were drilled perpendicular to the axis of the tunnels at stations 2+87 and 3+49. The holes, labelled MBI-7 and MBI-14, were drilled from one heater drift to the other, prior to mining of the canister drift. Therefore, four holes exist in the two pillars (Fig. 1): MBI-7N and MBI-7S (at station 2+87) and MBI-14N and MBI-14S (at station 3+49).

Altogether, 58 point measurements were made in the four holes, alternating vertical and horizontal directions; this averages about seven measurements per hole, per direction. Since the holes were 5.4 m long, the measurements were taken about every 38 cm. For an assumed Poisson's ratio $\nu = 0.25$, the modulus E is calculated as:

$$E_{calc} = 1.10 \cdot \Delta Q \cdot \frac{D}{\Delta D} ,$$

where ΔQ is the increment of hydraulic pressure in the jack and ΔD is the change in borehole diameter D. The E_{calc} is then used to obtain E_{true} as indicated in Fig. 7, which is derived from Ref. 9.

The results are summarized in Figs. 8a through d, which show the variation of the calculated field modulus through the thickness of the north and south pillars at stations 2+87 and 3+49, respectively. In addition, the rock quality designation (RQD) obtained from the same holes (MBI-7 and MBI-14) is also displayed.

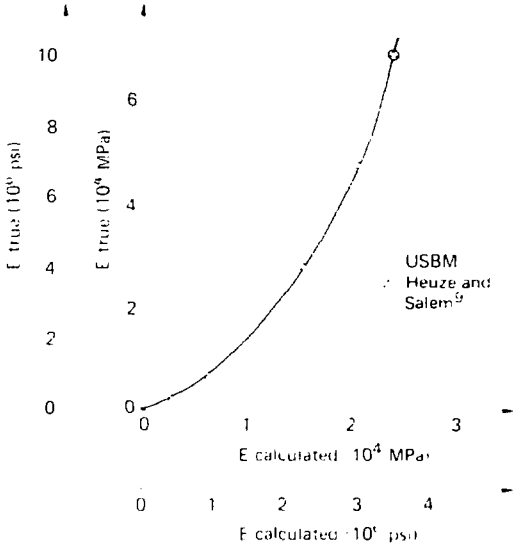

FIG. 7. Calibration curve for the NX-borehole jack; calculated vs true rock modulus (data from Heuze and Salem[9]).

RQD was first proposed by Deere.[11] It is defined from NX-core drilling (7.5-cm diameter hole) as the ratio

$$\text{RQD} = \frac{\text{sum of length of core pieces with length} \geq 10 \text{ cm}}{\text{total length drilled}} .$$

The mean value of this RQD is 80%. Note that this corresponds to a time before the center drift was excavated. The calculated E values do reflect the rock damage created in the rock mass near the walls of the drifts by the excavation process.

The results obtained in the south pillar are shown in Figs. 8a and b. Most E values range from 10 to 30 GPa (1.5 to 4.5 • 10^6 psi). The horizontal stiffness is somewhat lower than the vertical one in hole MBI-7 (station 2+87), but altogether, the south pillar stiffness seems to be fairly isotropic.

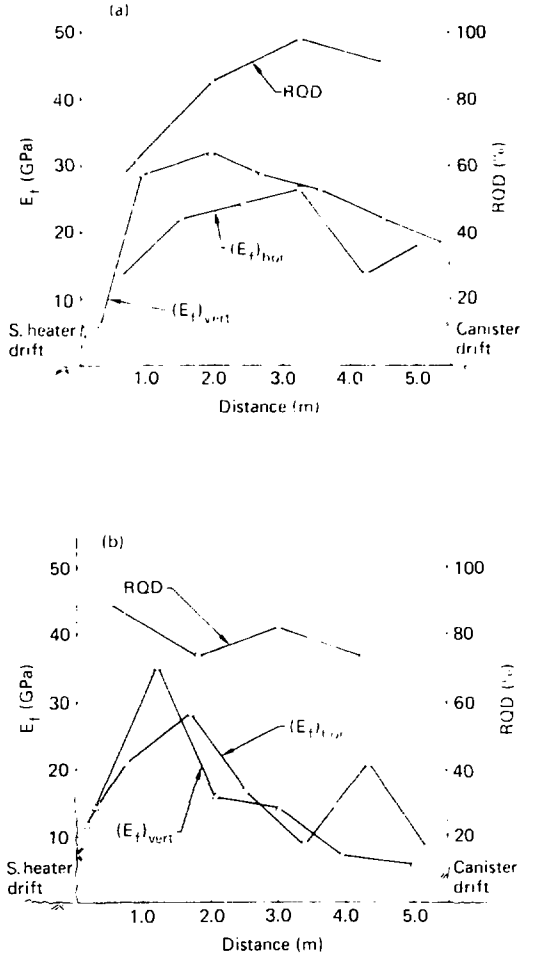

FIG. 8. In situ modulus and RQD, south pillar: (a) Hole MBI-7, station 2+87. (b) Hole MBI-14, station 3+49.

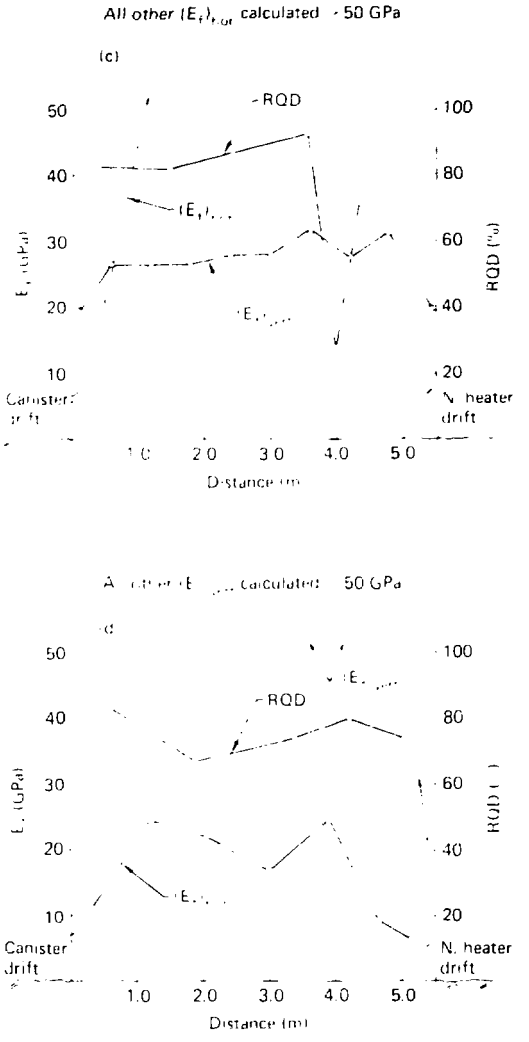

FIG. 8 (Continued). In situ modulus and RQD, north pillar: (c) Hole MBI-7, station 2+87. (d) Hole MBI-14, station 3+49.

Half of the results obtained in the north pillar (Figs. 8c and d) are consistent with the south pillar values. However, two sets of readings (E horizontal at station 2+87 and vertical at station 3+45) seem to give high E values that are not confirmed by other observations. It is likely that these high values are due to difficulty in seating the instrument in the hole because of a mismatch between hole and plate radius and because of joint movements into the borehole. For the purpose of modeling, we will adopt values in the range of 10 to 30 GPa as obtained in six of the eight series of stiffness measurements.

2.1.3 Discussion

Following the field work, the rented NX-jack was tested in a 7.5-cm hole bored at mid-height of a 35-cm cube of aluminum. It was found by inspection that for hydraulic pressures up to 60 MPa, the contact angle between the plates and the hole was about 31° instead of the nominal 90°. Using the 31° figure and applying both the corrections by Heuze and Salem[9] for longitudinal jack bending and by Hustrulid[10] for radius mismatch, enabled us to make a satisfactory calculation of the modulus of the aluminum block, comparable to that obtained independently.

However, the true plate contact cannot be obtained in rock boreholes at a depth beyond a few inches. In the less compliant rocks, the plate may not seat correctly, and the jack will measure a lower bound for the modulus. Accordingly, we are now considering a redesign of the basic NX-jack to eliminate the effects of both longitudinal bending and radius mismatch on the measurements. This would enable us to dispense with any correction factor in data analysis.

2.2 MODIFIED NX-BOREHOLE JACK TESTS

2.2.1 Principle of the Test

De la Cruz has developed a modified version of the NX-jack.[12] Its principle of measurement is illustrated in Fig. 9.

As before, the wall of the borehole is loaded by steel plates covering two 90° arcs. However, the modulus measurement is no longer based on monitoring a change in borehole diameter in the direction of loading. Instead, a pair of

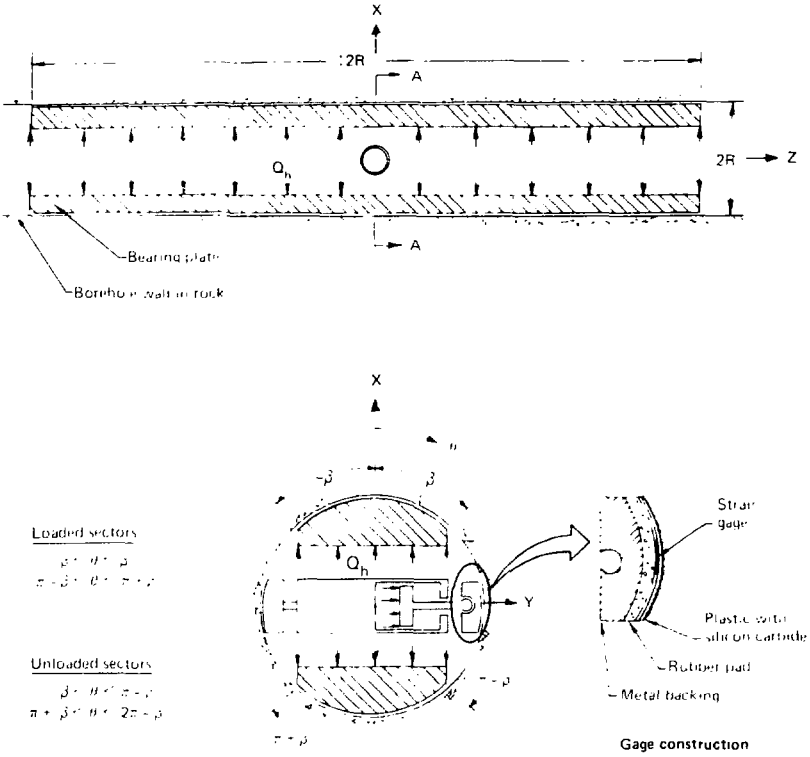

Sec. A-A' Transverse cross section

R – radius of borehole
Q_h – uniform unidirectional pressure

FIG. 9. Principle of the modified NX-borehole jack test (data from De la Cruz[12]).

friction strain gages are installed at 90° to the direction of loading; i.e., Θ = 0 and 180° on Fig. 9. With

R = hole radius,

Q_h = hydraulic pressure behind the plates,

A_h = plate area,

the tangential stress $\sigma_{\theta\theta}$ at points A and B is

$$\sigma_{\theta\theta} = \frac{1}{2} \frac{A_h \cdot Q_h}{R} \quad ,$$

and for this particular instrument and hole size

$$\sigma_{\theta\theta} = 0.625\ Q_h \quad .$$

The plate length has been extended to 45 cm, as opposed to 20 cm for the original jack. With a 7.5-cm diameter hole, the loading can be assumed to be close to a plane strain condition. Hence, the tangential strain $\varepsilon_{\theta\theta}$ at A and B can be found as:

$$\varepsilon_{\theta\theta} = \frac{1 - \nu^2}{E} \sigma_{\theta\theta} \quad .$$

Therefore, the modulus E can be finally expressed as

$$E = 0.625\ (1 - \nu^2)\ \frac{Q_h}{\varepsilon_{\theta\theta}} \quad .$$

For a Poisson's ratio assumed to be ν = 0.25,

$$E = 0.59\ \frac{Q_h}{\varepsilon_{\theta\theta}} \quad .$$

2.2.2 Modified NX-Borehole Jack Tests at SFT-C

This last equation was used to analyze the data from 34 measurements in holes MBI-7 and MBI-14. The calculated values are summarized in Table 2. E is shown at values of Q_n where the record was linear. Two striking results emerge:

- The mean and standard deviation of the E modulus, measured in the damaged skin of the pillars, is

$$E = 87.1 \pm 20.0 \text{ GPa},$$

whereas the measurements away from this zone give

$$E = 66.7 \pm 16.6 \text{ GPa}.$$

- The lower value of 66.7 is as high as the values obtained on 2-in. diameter cores in the laboratory. This is contrary to all other evidence which shows the field moduli to be lower than the laboratory-measured values. Table 3 was extracted from Ref. 13 to illustrate this point.

2.2.3 Discussion

In spite of their oddity, the modified jack results are internally consistent and can be explained in terms of a breakdown in the assumptions on which the measurements are based. The calculations of E assume that the rock mass is continuous and isotropic. However, let a few fractures exist around the borehole as sketched in Fig. 10.

The medium is unable to transmit a high tensile strain at the $\theta = \pm 90°$ points, and $\sigma_{\theta\theta}$ is very small. This leads to calculating a very high E value, which is contrary to the physical reality. So it is not surprising that the E reported for the damaged pillar skin is higher than E inside the pillar. Even with the above shortcoming, the modified borehole jack should be useful for testing in massive rock such as is often found in thick sedimentary formations. The results of the original and the modified NX-jack will be compared further in Sec. 2.5.

TABLE 2. Summary of modulus values obtained with modified NX-jack.

Hole	Station	Depth from S collar (m)	Q_h (MPa)	$\epsilon_{\theta\theta}$ (10^{-6})	E (GPa)
MBI-7N	2+87	0.3	48.2	296	96.5[a]
		0.9	29.6	236	74.5
		1.5	34.5	470	43.4
		2.1	34.5	278	73.1
		2.7	24.1	243	42.0
		3.3	27.6	335	48.3
		3.9	34.5	348	58.6
		4.5	34.5	445	45.5
		5.1	34.5	383	53.1[a]
MBI-14N	3+49	0.3	23.0	222	61.4[a]
		0.9	46.2	416	65.5
		1.5	42.1	217	59.3
		2.1	53.8	610	51.7
		2.7	38.3	361	62.7
		3.3	45.9	295	91.7
		3.9	24.8	268	55.2
		4.5	41.4	400	61.4
		5.1	55.2	374	86.9[a]
MBI-14S	3+49	0.6	49.6	307	106.9[a]
		1.2	38.3	224	100.0
		1.8	34.5	247	82.7
		2.4	17.2	162	62.7
		3.0	61.4	357	86.9
		3.6	61.4	472	76.5
		4.2	23.0	195	69.6
		4.8	30.3	167	108.3[a]
MBI-7S	2+87	0.6	26.8	170	92.4[a]
		1.2	26.8	200	75.9
		1.8	42.1	522	47.6
		2.4	42.1	333	74.5
		3.0	42.1	323	76.5
		3.6	42.1	365	67.6
		4.2	23.0	222	61.4
		4.8	34.5	222	91.7[a]

[a]Values calculated for the damaged rock in the skin of the pillars.

TABLE 3. Ratio of field modulus (E_f) to laboratory modulus (E_ℓ) for granitic rocks (data from Heuze[13]).

Location	Rock type	Type of test										
		PB	TR	FJ	PC	GJ	FM	BT	BC	PS	RM	QR
Tumut	Granite gneiss	0.12	0.12	0.97	0.30							
Dworshak	Granite gneiss	0.45				0.45						
LG-2	Granite	0.62										
Gage D	Granite	0.13	0.66				0.66					
Auburn	Granite gneiss	0.35			0.31							
Montezic	Granite	0.14										
Montezic	Granite	0.85										
Machu Picchu	Granodiorite							0.47				
Mantari III	Granite							0.21				
Stripa	Granite								0.54			
Climax/NTS	Quartz monzonite					0.36				0.67	0.38	0.36

Legend

PB: Plate bearing or uniaxial jack
TR: Tunnel relaxation
FJ: Flat jack
PC: Pressure chamber
GJ: Goodman Jack
FM: Foundation movement
BT: Block test
BC: Borehole pressure cell
PS: Petite sismique
RMR: Rock mass rating prediction
QR: Q-rating

Note: Average ratio E_f / E_ℓ (20 test series): 0.44 ± 0.24.

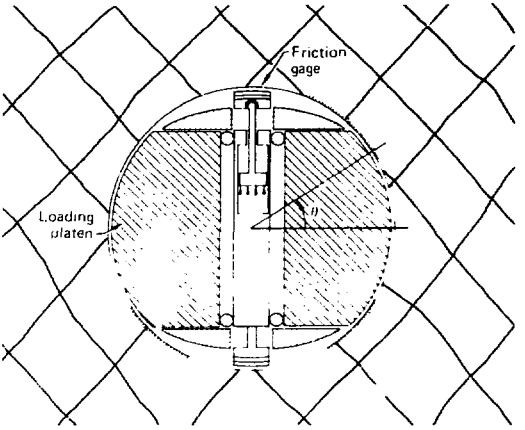

FIG. 10. Modified NX-borehole jack loading in fractured rock mass [40]

2.3 PETITE SISMIQUE TESTS

2.3.1 The Petite Sismique Method

The petite sismique method is an indirect technique used to estimate the field modulus of rock masses. First proposed in 1967 by Schneider,[14] only a few additional studies have been reported, those by Bieniawski.[15] This method consists of measuring the frequency of first arrivals of horizontally polarized shear waves propagated through the rock mass. The shear-wave frequency, (N), is empirically related to the field modulus.[14,15] This is based upon the measurements of N by petite sismique and of E by plate tests at a number of sites worldwide (Fig. 11). Figure 11 was extracted from the results by Schneider and Bieniawski; it displays only the points corresponding to igneous rocks. Note that Schneider's results are between 250 and 600 Hz, and Bieniawski's are between 450 and 950 Hz. The two sets of data seem to correlate very well.

So, at the outset of our work at Climax, it appeared that the petite sismique would be a very promising tool to obtain the modulus of the granite, on a large scale, without the considerable expense involved in large plate tests.[16]

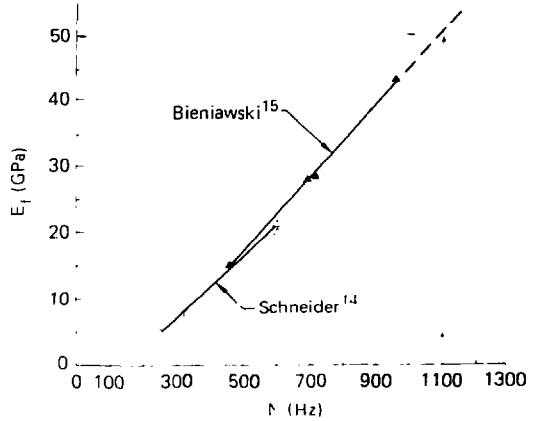

FIG. 11. Empirical correlation between shear wave frequency (N) and static modulus of igneous rock masses.

2.3.2 Petite Sismique Tests at SFT-C

After a survey of manufacturers, we decided to use a Nimbus model ES-125 dual-channel signal-enhancement seismograph tied to an ESR-100 strip chart recorder. We rented the equipment from Geometrics in Sunnyvale, California. The main accessories were an HS-3 solid state hammer switch and three GH-3-14 horizontal geophones.

The layout of the tests is shown in Fig. 12. The six geophone stations were put on the walls of the center drift. For source points we used a variety of configurations. Finally, we settled upon anchored rock bolt plates, rapped sideways with a 4-lb hammer. The source points were all in the heater drifts.

We successfully completed the 12 traverses shown in Fig. 12; records of the results are given in part "a" of Figs. 13-15. The results were obtained with two or four hits; their quality was enhanced by reversing the polarity and the striking direction on alternate blows. This effectively minimized the P-wave contribution.

Table 4 summarizes the values calculated for the apparent shear-wave frequency (N). As the records show, N is quite constant over several wave lengths. The method was successfully applied to distances up to 25 m. Hence,

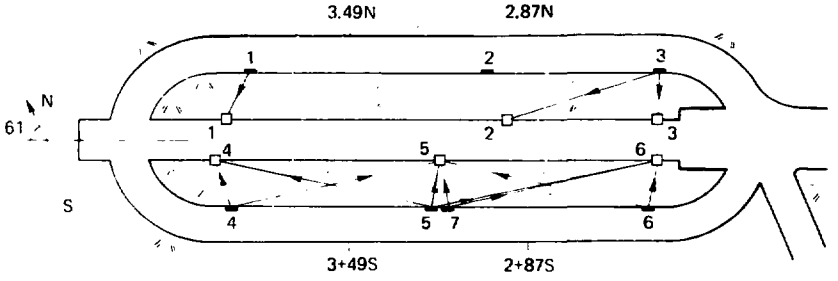

FIG. 12. Layout of the petite sismique traverses at SFT-C.

the volume of rock involved in the test is very large, compared to that in any borehole jack or plate test. The only failure of the system was in the triggering, which was not reliable enough to permit calculation of velocities. However, the petite sismique method deals with frequencies, not velocities.

The mean values of the apparent N were calculated as:

$$\text{North pillar } N = 1{,}168 \pm 73 \text{ Hz},$$
$$\text{South pillar } N = 1{,}061 \pm 105 \text{ Hz}.$$

The 10% difference in the mean may be due to a higher degree of fracturing in the south pillar. This would be consistent with other indications such as the difficulties in performing jack-fracturing stress measurements, as discussed in the section on in situ stresses.

2.3.3 Discussion

To refine our analysis, we digitized the records shown in part "a" of Figs. 13-15 and produced power spectra. These are shown in part "b" of Figs. 13-15. The peak frequencies for the various traverses are summarized in Table 5.

When the values of the apparent N given in Sec. 2.3.2 are entered into Fig. 11, they indicate a modulus of about 50 GPa in the rock pillars. This is

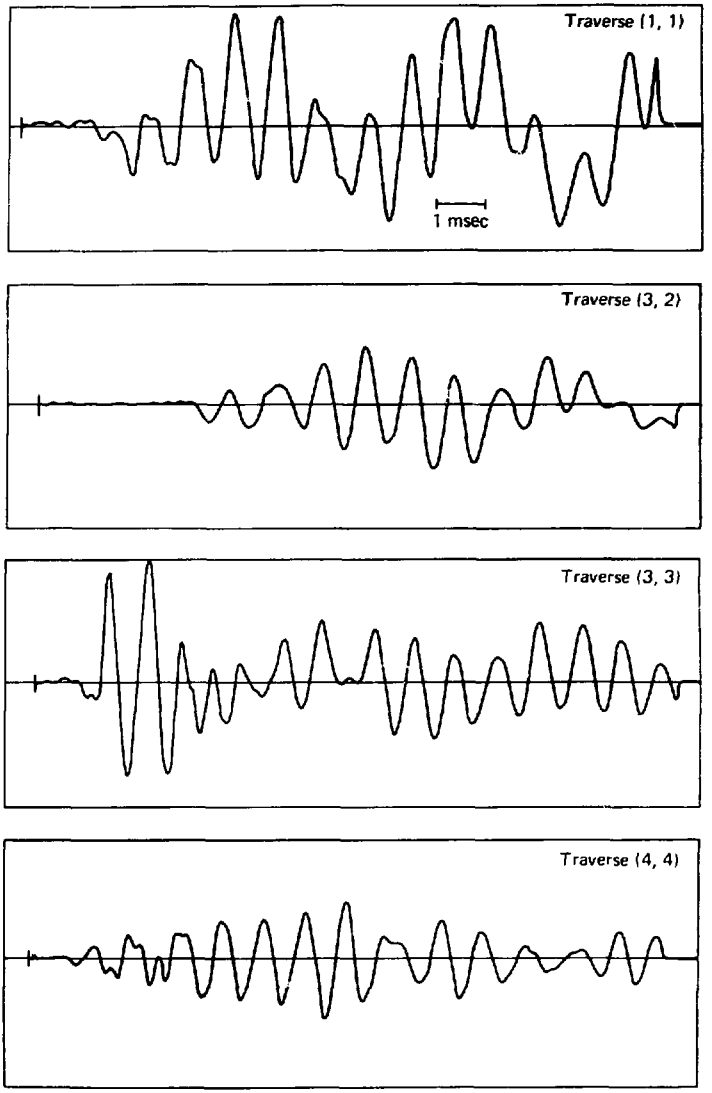

FIG. 13. (a) Records of shear wave arrivals at SFT-C (traverses 1,1; 3,2; 3,3; 4,4).

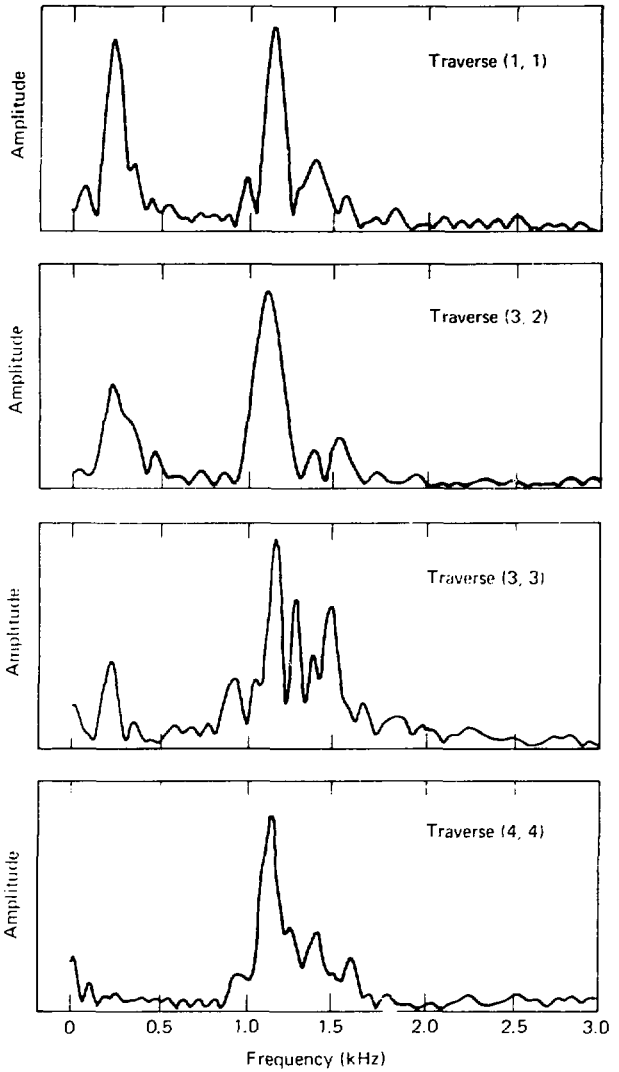

FIG. 13. (b) Power spectra that correspond to the wave records of Fig. 13a.

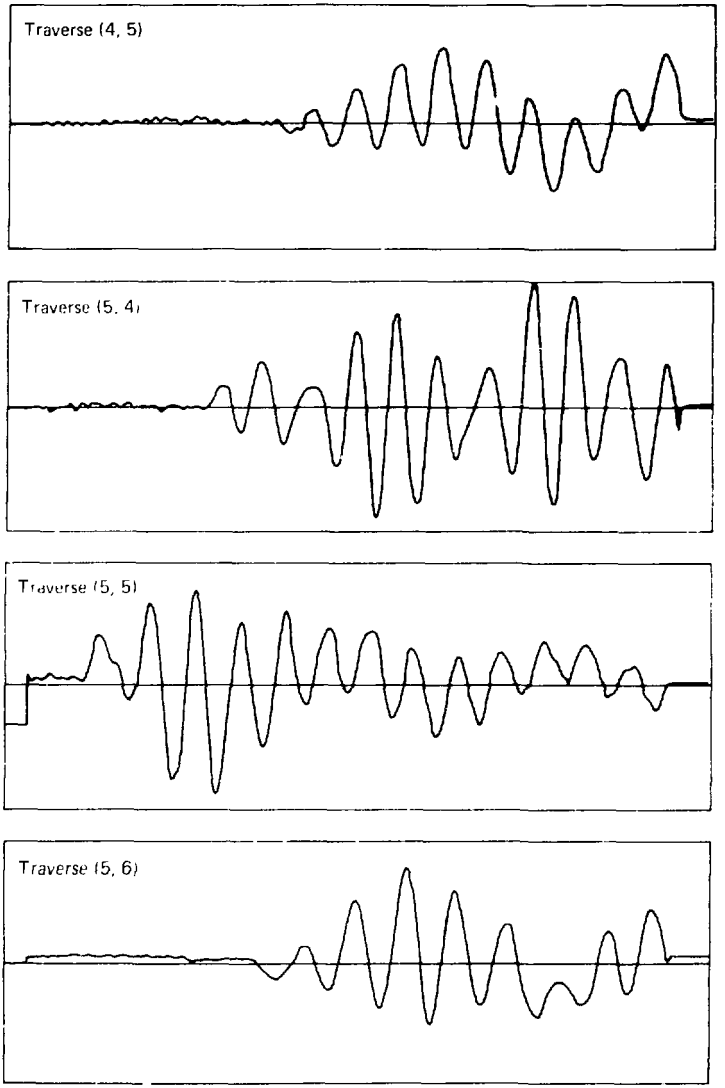

FIG. 14. (a) Records of shear wave arrivals at SFT-C (traverses 4,5; 5,4; 5,5; 5,6).

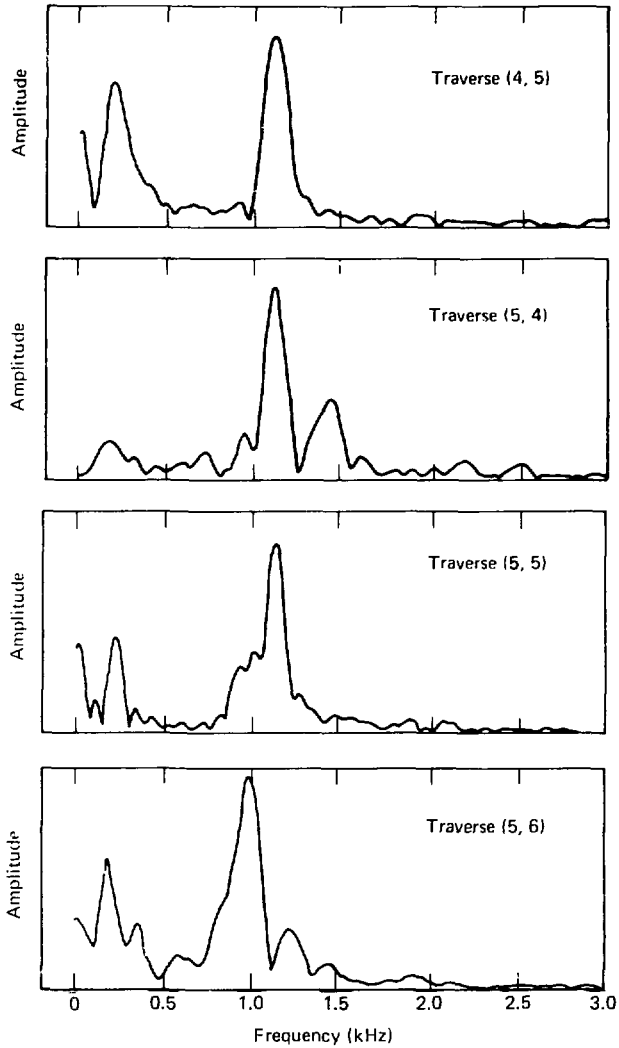

FIG. 14. (b) Power spectra that correspond to the wave records of Fig 14a.

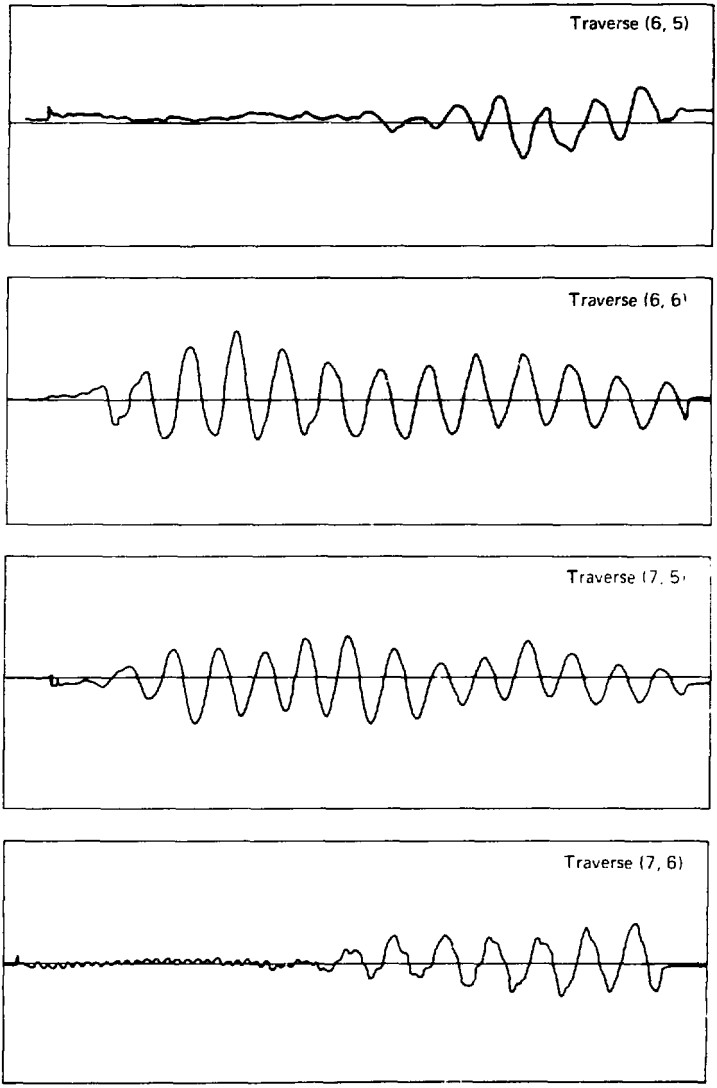

FIG. 15. (a) Records of shear wave arrivals at SFT-C (traverses 6,5; 6,6; 7,5; 7,6).

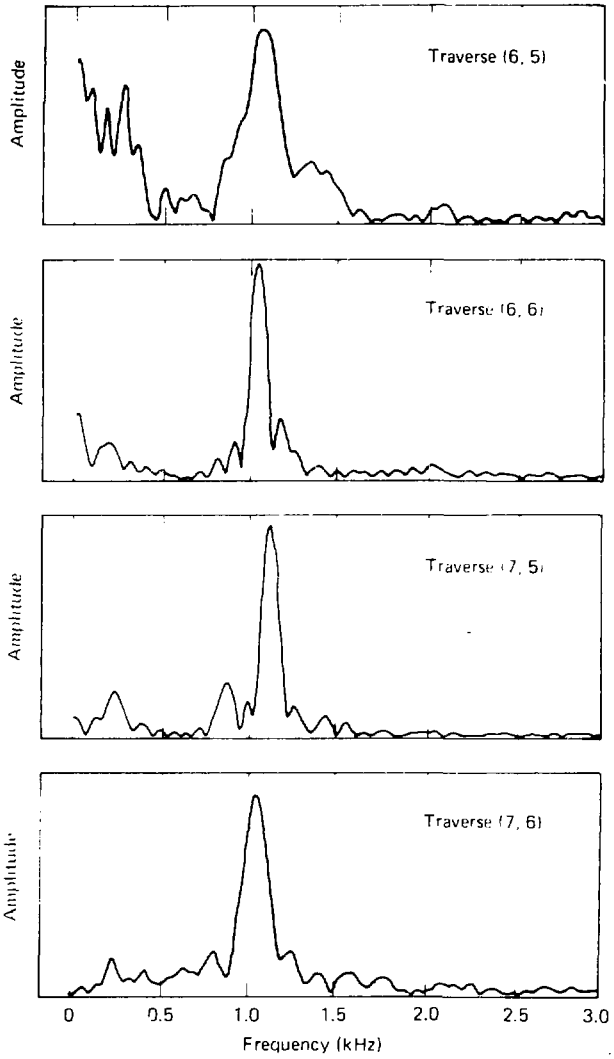

FIG. 15. (b) Power spectra that correspond to the wave records of Fig. 15a.

TABLE 4. Preliminary analysis of petite sismique results at SFT-C.

Traverse (Fig. 16	Length (m)	Apparent period (ms)	Apparent frequency (Hz	Average apparent frequency (Hz
(1,1)	5.4	0.85-0.90	1,143	
(3,2	19.2	0.90	1,111	1,169 ± 73
(3,3	5.4	0.80	1,250	
(4,4	5.7	0.85	1,176	
(4,5	18.9	0.85	1,176	1,176
(5,4	20.4	0.85	1,176	
5,5	5.4	1.00-1.07	952	917 ± 58
5,6	24.6	1.05-1.25	869	
6,5	23.1	0.95	1,050	
(6,6	5.7	0.95	1,053	
7,5	5.4	0.9-1.0	1,100	
(7,6	22.5	0.95	1,053	

TABLE 5. Summary of petite sismique results at SFT-C.

Traverse (Fig. 6)	Pillar	Length (m)	Peak frequency (Hz)
(1,1)	North	5.4	1,140
(3,2)	North	19.2	1,000
(3,3)	North	5.4	1,150
(4,4)	South	5.7	1,100
(4,5)	South	18.9	1,100
(5,4)	South	20.4	1,090
(5,5)	South	5.4	1,120
(5,6)	South	24.6	960
(6,5)	South	23.1	1,040
(6,6)	South	5.7	1,030
(7,5)	South	5.4	1,120
(7,6)	South	22.5	1,030

definitely too high a number, based on the other measurements at Climax and elsewhere (Table 3). Hence, we may find out as we develop more data that the universal relation proposed between N and E is not to be taken without reservation. A personal communication with Bieniawski regarding his recent tests in a limestone quarry confirms this.

2.4 OTHER ESTIMATES OF ROCK-MASS DEFORMABILITY

In this section we present deformability estimates based on three additional approaches:

- Bieniawski's rock mass rating.[17]
- Barton's Q-system.[18]
- Models of tunnel relaxation.[1,3]

2.4.1 Estimate Based on Rock Mass Rating (RMR)

The RMR rating, proposed by Bieniawski,[17] varies between 0 and 100. It is heavily dependent upon the geometry and properties of fractures. Bieniawski has proposed an empirical relationship between RMR and in situ modulus, based on several projects where field measurements were performed. This relationship is illustrated in Fig. 16.

When this approach is applied to Climax, the following ratings are obtained:

Parameter		Range of values
Intact rock uniaxial strength (100-250 MPa)		12 - 12
RQD (75-90%)		17 - 17
Spacing of discontinuities (0.2-0.6 m)		10 - 10
Condition of discontinuities		25 - 30
Ground water		10 - 15
Adjustment for joint orientation		-10 - -5
	Total	64 - 79

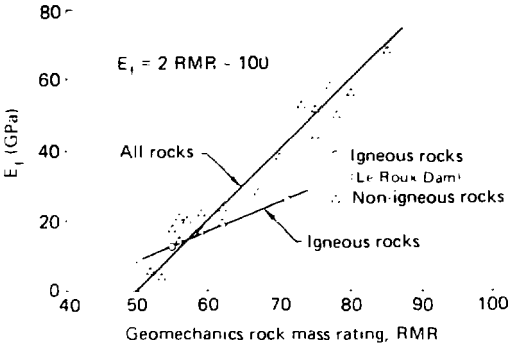

FIG. 16. Empirical correlation between RMR and in situ modulus of rock masses (data from Bieniawski[17]).

According to Fig. 16, the modulus in place could be expected to be in the range of

$$28 \text{ GPa} \leq E_f \leq 58 \text{ GPa} ,$$

with a mean value of

$$E_f = 43 \text{ GPa} .$$

With an intact rock modulus of E_ℓ = 70 GPa, this would mean a modulus reduction factor E_f / E_ℓ = 0.62, which is quite high when compared with the results shown in Table 3 for other granitic sites.

However, we can take a closer look at Fig. 16. The types of rocks on the various projects are listed in Ref. 15. Of these, only the Le Roux Dam rocks are igneous, as is granite. A line through the two corresponding data points shows that the E values corresponding to RMRs of 64 and 79 are 20 and 32 GPa, respectively. The mean is

$$E_f = 26 \text{ GPa} ,$$

corresponding to a modulus reduction factor E_f / E_ℓ = 0.38. Admittedly, the above calculation is based on a very small data base and assumes that

different (RMR, E) relations exist for different classes of rock. However, the last estimate is more consistent with other results for granite (Table 3) and with the direct measurements at Climax. As the RMR data base expands, it can be refined, and it is likely to become more useful.

The RMR rating is not to be confused with the rock structure rating (RSR), which has been proposed by Wickham and Tiedemann.[19] The RSR again depends heavily upon fracture properties. Both the RMR and RSR classifications were developed originally to provide guidelines for the support requirements of rock caverns. However, no correlation between RSR and modulus has been reported in the literature.

2.4.2 Estimate Based on the Q-system

The Q classification, proposed by Barton et al.,[18] is based on a rating calculated as

$$Q = \frac{RQD}{J_n} \cdot \frac{J_r}{J_a} \cdot \frac{J_w}{SRF} ,$$

where:

RQD = rock quality designation,
J_n = joint set factor,
J_r = joint roughness factor,
J_a = joint alteration factor,
J_w = joint water reduction factor,
SRF = stress reduction factor.

Specifically, at the SFT-C site, the range of parameters can be estimated as:

Parameter	Range of values
RQD:	75 - 90
J_n : 3 sets of joints	9 - 9
J_r : rough, fairly planar joint	1.5 - 1.5
J_a : unaltered to slightly altered with surface staining	1 - 1.5
J_w : dry or minor inflow	1 - 1
SRF: medium stress with a few weakness zones containing clay	1 - 2

so that the range of Q is

$$4.2 \leq Q \leq 15 ,$$

giving a mean value of Q = 9.6.

Barton[18] has presented an empirical relation between Q and the field modulus (Fig. 17). From Q = 9.6 we would estimate the in situ modulus as:

$$E_f = 26 \text{ GPa} ,$$

corresponding to a modulus reduction factor $E_f / E_l = 0.38$. Again, it is seen that the data base from which this estimate is taken is small. There is no reference to rock classes in Fig. 17, but it is believed that most of the results came from granitic rocks around caverns in Scandinavia.

2.4.3 Estimate Based on Models of Tunnel Relaxation

If numerical modeling is performed in conjunction with field measurements of rock-mass deformations, the models can provide an indirect way of back-calculating rock-mass stiffness. Based on the two calculations previously reported,[1,3] it appears that a rock-mass modulus in the range of

$$20 \text{ GPa} \leq E_f \leq 32 \text{ GPa}$$

could provide reasonable agreement between observed and predicted rock movements away from the immediate vicinity of the tunnels.

2.5 COMPARISON OF MODULUS ESTIMATES

The range of values for the six types of rock-mass deformability estimates is summarized in Fig. 18.[1] The laboratory moduli reported by three different sources are also shown.[2,20,21] The high E_f values provided by the modified NX-jack are explained in Sec. 2.2.3.

Through the use of multiple techniques, it appears that a reasonable estimate of the stiffness of the Climax granite in the field can be put at

$$20 \text{ GPa} \leq E_f \leq 32 \text{ GPa} ,$$

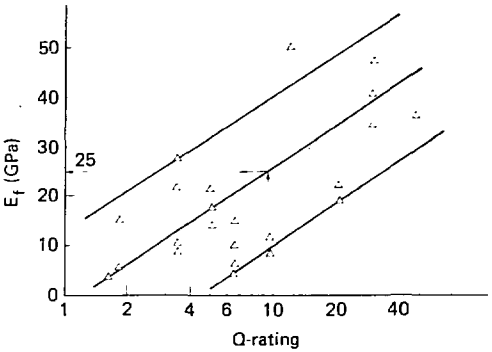

FIG. 17. Empirical correlation between Q-rating and in situ modulus of rock masses (data from Barton et al.[18]).

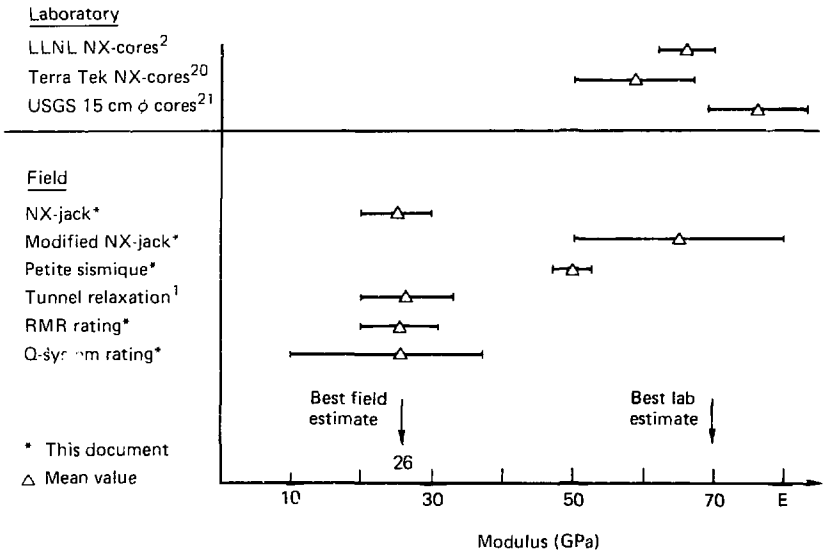

FIG. 18. Multiple estimates of laboratory and field modulus for Climax granite.

with a mean best estimate of

$$E_f = 26 \text{ GPa} .$$

For a mean laboratory estimate of E_ℓ = 70 GPa, this corresponds to a modulus reduction factor of

$$E_f / E_\ell = 0.37 ,$$

which is compatible with the mean of the results in Table 3.

3. IN SITU NORMAL STIFFNESS OF CLIMAX GRANITE JOINTS

We recall that at Climax the three sets of joints have about the same spacing and are nearly perpendicular to each other. This suggests the feasibility of testing an equivalent-continuum model to represent the deformability of the rock mass. Such an approach has been used successfully in a tri-jointed marble.[22,23] The modulus of the equivalent continuum is the same along the three principal strain directions, which are perpendicular to the three joint directions. The representative modulus is

$$E_f = \frac{1}{\frac{1}{E_\ell} + \frac{1}{sK_n}} = \frac{E_\ell \cdot s \cdot K_n}{E_\ell + s \cdot K_n} ,$$

where

E_ℓ = modulus of the intact rock blocks,
s = mean joint spacing,
K_n = normal joint stiffness.

The above equation is represented graphically in Fig. 19 for a range of values of s and K_n, which, thus, give different values of E_f / E_ℓ. The curves are drawn for E_ℓ = 70 GPa; we consider this the best estimate for the modulus of intact Climax granite (Fig. 18).

In the present case, the unknowns are s, E_f, and K_n. If s and K_n are known, the field modulus E_f can be calculated. The s could be measured

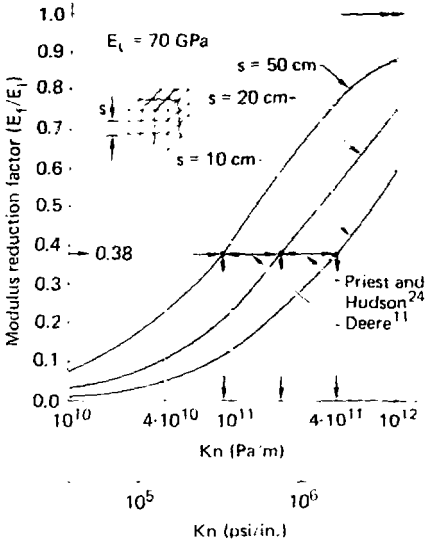

FIG. 19. Variation of modulus reduction factor with joint spacing and normal joint stiffness for a rock mass with three orthogonal sets of joints.

directly or estimated from calculated values of RQD. Both Deere[11] and Priest and Hudson[24] have proposed correlations between s and the RQD, as shown in Fig. 20. The relation proposed by Deere is empirical, whereas that from Priest and Hudson is based on an analytical expression, assuming randomly spaced discontinuities. For NX-cores the Priest/Hudson formula for the estimated RQD is

$$RQD = 100 \cdot e^{-0.1\lambda} (0.1\lambda + 1) ,$$

where λ is the average number of discontinuities per metre.

This estimate has been tested by Wallis and King[25] in a granite with an RQD of between 86 and 98%. The estimated and calculated values were within 2% of each other. On the other hand, the Deere relation was confirmed by Heuze in a marble with three orthogonal joint sets.[22]

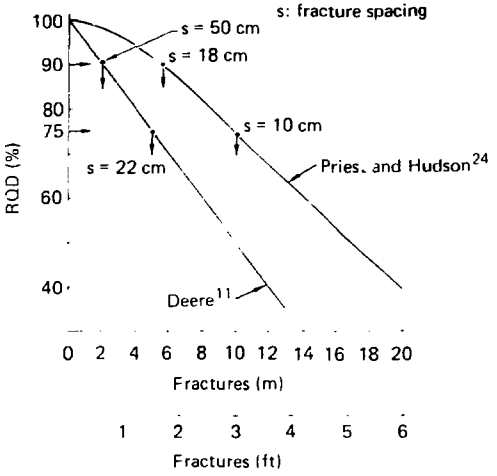

FIG. 20. Proposed correlations between RQD and fracture spacing.

The problem is that even if s is determined, there is not currently any field test designed to measure the normal joint stiffness, K_n. K_n values have been reported from laboratory tests on natural joints, but we do not know whether, due to possible scale effects,[26] these values are representative of field situations. One can conceive a type of dual flat-jack test to measure K_n, but this has not been implemented at Climax or elsewhere to our knowledge. Such a test should be attempted. We also note that K_n is a critical parameter in the modeling of fluid flow in fractured media.[27-29]

We could turn the problem around and assume that s and E_ℓ are known; then one can obtain estimates for K_n. Let us assume that the granite at Climax has a mean modulus E_f = 26 GPa. Using the information in Fig. 20 with the RQD values between 75 and 90%, we would estimate fracture spacing as:

$$10 \text{ cm} \leq s \leq 20 \text{ cm (after Deere)},$$

$$18 \text{ cm} \leq s \leq 50 \text{ cm (after Hudson and Priest)}.$$

In turn, we can go back to Fig. 19 and find that for the two ranges of estimates that are nearly contiguous

$$9 \cdot 10^{10} \text{ Pa/m} \leq K_n \leq 2 \cdot 10^{11} \text{ Pa/m (after Deere)},$$

$$2 \cdot 10^{11} \text{ Pa/m} \leq K_n \leq 4 \cdot 10^{11} \text{ Pa/m (after Hudson and Priest)},$$

Note: $2.7 \cdot 10^{11}$ Pa/m = 10^6 psi/in.

The laboratory-measured values of K_n reported in the literature are usually smaller than 10^6 psi/in. They also exhibit a strong nonlinear dependency upon the normal stress acting on the joint.[27,29] However, there is no data base for field-measured normal stiffness. Thus, it is very difficult to choose between the RQD vs s relation proposed by Deere and that by Hudson and Priest. Both for the purpose of estimating the stiffness of rock masses and for modeling fluid flow in rock fractures, it appears very desirable to measure the normal stiffness of joints in place.

4. IN SITU STRESSES

Three campaigns of stress measurements have been performed in the Climax granite since 1979:

- Overcoring tests by Ellis of the U.S. Geological Survey (USGS) in one hole plunging 77° (OC-1) and two near-horizontal holes (OC-2 and OC-3), all drilled from the south heater drift.[21,30,31]
- Undercoring tests by Heuze and Patrick at six locations in the heater drifts (pillar, crown, and abutment in each drift).
- Borehole jack fracturing tests by De la Cruz and Voss in holes MBI-7 and MBI-14.

The locations of these measurements are shown on Fig. 21. Note that all the tests were conducted in the central portion of the heater drifts or pillars.

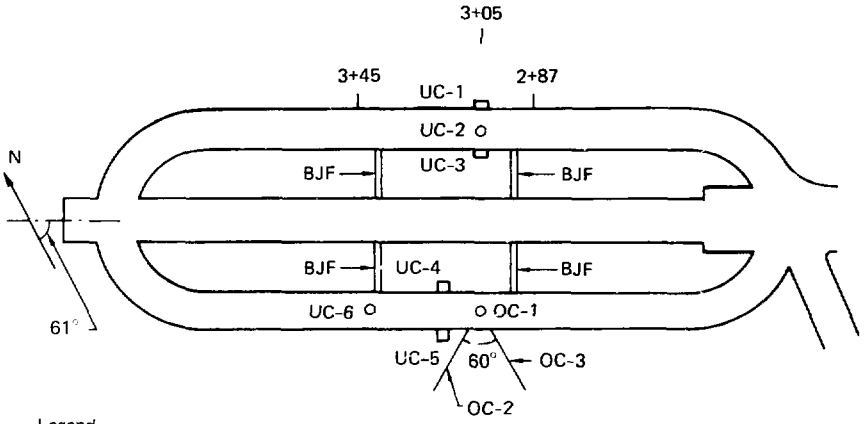

Legend
BJF: Borehole jack fracturing
OC: Overcoring, USBM gage
UC: Undercoring, surface rosette

FIG. 21. Location of stress measurements at SFT-C made during 1979-80.

4.1 PREVIOUS STRESS MEASUREMENTS BY THE USGS

4.1.1 Reported Stress Values

The USGS used overcoring of a three-component borehole gage[32] to estimate stresses around the south heater drift. Four measurements were made in holes 1 and 3, to a depth of 6 to 7 m; eleven measurements were made in hole 2, to a depth of 5.3 m. The deepest readings in the three holes were combined to produce a calculation of three principal stresses (σ_1, σ_2, and σ_3) away from the drift, according to a least square regression procedure.[33-35]

The reported values[21] are summarized in Table 6. The first stress invariant is I_1 = 21.44 MPa. The virgin vertical stress calculated from σ_1, σ_2, and σ_3 is reported as σ_v = 7.92 MPa. Assuming a lithostatic burden, it is only 73% of the expected value of 10.9 MPa.

The difference should be even greater if one considers that the rock modulus used to analyze the overcoring data was taken as 77 GPa from tests on 15-cm diameter cores. Such a value is about 10% in excess of the best

TABLE 6. Principal stresses reported by the U.S. Geological Survey, using overcoring method (data from Ellis[21]).

Component		Value		Bearing	Plunge[a]
		MPa	psi		
σ_1	(maximum)	11.56	1676	N56E	-29°
σ_2		7.13	1034	N26E	$+57^{\circ}$
σ_3	(minimum)	2.75	399	N42W	-14°

[a]Negative plunge is below the horizontal plane.

estimate reported in Fig. 20. This probably is due to the fact that the cylindrical loading of the cores in a hydraulic pressure cell tends to yield high modulus values.[22] In such a cell the core is not subjected to uneven lateral stresses, as usually occurs in situ. In other words, bulk compression will give a higher modulus than when shear deformation can occur. Thus, the reported σ_v value should be decreased by at least 10%, making it 65% of overburden, at the most.

Moreover, the overcoring holes may have stopped short of going the length required to reach a region of undisturbed original stresses. From current numerical models,[4] we estimate that this minimum distance could reach over 9 m, depending upon the pattern of joints and shears. The models also show that, short of this depth, stress values will be higher than the undisturbed ones.

4.1.2 Discussion of Horizontal and Vertical Stresses

The above ratio of horizontal-to-vertical stress is quite unusual when compared to values reported in the literature. For completeness we calculated the virgin horizontal stresses perpendicular and parallel to the axis of the tunnels, and we verified the calculated value of the virgin vertical stress with the help of the stereonet.[36]

Start with the virgin horizontal stress, σ_{h1} perpendicular to the axis of the tunnels in the general vicinity of the overcoring measurements. It is the normal stress across a vertical plane, striking N61W (Fig. 21). We will call π_1 the trace of the normal to this plane on the stereonet (Fig. 22a).

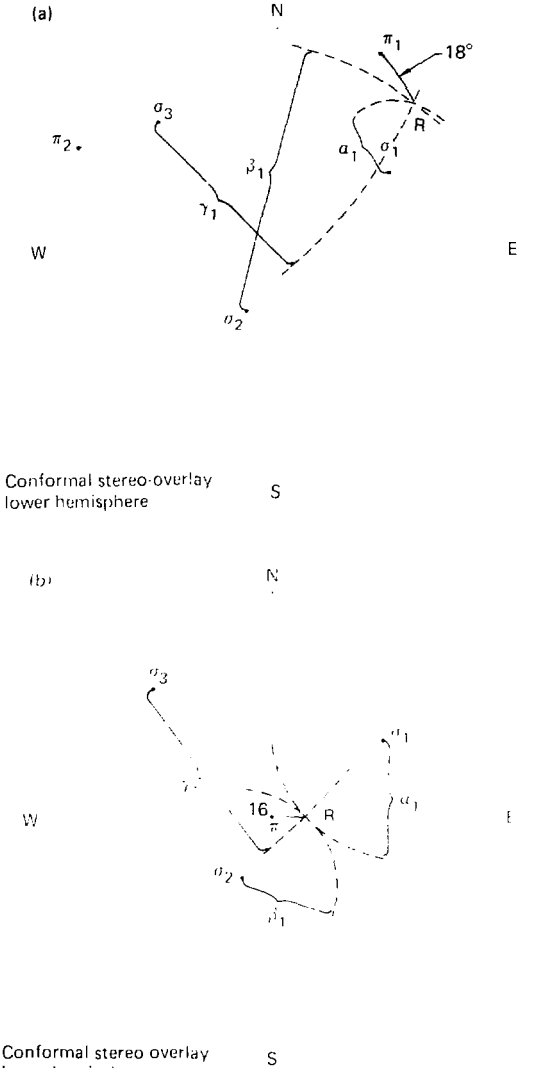

FIG. 22. Principal stresses at SFT-C and resultant (R): (a) across vertical plane striking N61W. (b) across horizontal plane striking N29E.

To obtain a right-handed (σ_1, σ_2, σ_3) coordinate system, we have to use the opposite direction for σ_2 to the one given by Ellis.[21] When the angles α, β and γ between the direction of π_1 and the directions of σ_1, σ_2, and σ_3 are measured on the stereonet, the direction cosines of π_1 become:

$$l = \cos \alpha = \cos 40^\circ = .766$$
$$m = \cos \beta = \cos 57^\circ = .544$$
$$n = \cos \gamma = \cos 70^\circ = .342$$
$$(l^2 + m^2 + n^2 = 0.9997 \simeq 1.0)$$

The magnitude R of the resultant stress across the plane striking N61W is

$$R = \left(l^2 \sigma_1^2 + m^2 \sigma_2^2 + n^2 \sigma_3^2 \right)^{1/2} = 9.71 \text{ MPa} .$$

Now the direction cosines of the resultant R are

$$\cos \alpha_1 = \frac{l\sigma_1}{R} \qquad \cos \beta_1 = \frac{m\sigma_2}{R} \qquad \cos \gamma_1 = \frac{n\sigma_3}{R}$$

$$\cos \alpha_1 = .912 \qquad \cos \beta_1 = .399 \qquad \cos \gamma_1 = .097$$

$$(.9122 + .3992 + .0972 = 1.0003 \simeq 1.0) .$$

From these the angles between R and the σs become

$$\alpha_1 = 24^\circ, \qquad \beta_1 = 66.5^\circ, \qquad \gamma_1 = 84.5^\circ.$$

By drawing the corresponding cones about the directions of σ's, the direction of R is located on the stereonet at the intersection of the three cones. The great circle through R and π_1 corresponds to the plane containing the normal π_1 and the resultant R. The angle between R and σ_1 is read as 18°. Thus, the normal stress on the vertical plane striking N61W is

$$\sigma_{h1} = \cos 18^\circ = 9.23 \text{ MPa} .$$

Knowing l, m, and n, an alternate calculation is

$$\sigma_{h1} = l^2 \sigma_1 + m^2 \sigma_2 + n^2 \sigma_3 = 9.22 \text{ MPa} \quad .$$

The same procedure can be applied to verify the value of σ_v reported by Ellis.[21] The construction is shown on Fig. 22b. The normal to the horizontal plane is called π. Then

$$l = \cos \alpha = \cos 61^\circ = .485$$
$$m = \cos \beta = \cos 33^\circ = .838$$
$$n = \cos \gamma = \cos 76^\circ = .242$$
$$(l^2 + m^2 + n^2 = 0.996 \simeq 1.0)$$

$$R = l^2 \sigma_1^2 + m^2 \sigma_2^2 + n^2 \sigma_3^2 = 8.22 \text{ MPa} \quad .$$

$$\cos \alpha_1 = \frac{l\sigma_1}{R} = .682 \ , \ \cos \beta_1 = \frac{m\sigma_2}{R} = .727 \ , \ \cos \beta_1 = \frac{n\sigma_3}{R} = .081 \quad ,$$

$$(.682^2 + .727^2 + .081^2 = 1.002 \simeq 1.0) \quad .$$

$$\alpha_1 = 47.0^\circ, \qquad \beta_1 = 43.5^\circ, \qquad \gamma_1 = 85.5^\circ \quad ,$$

so that $\sigma_v = 8.22 \cos 16^\circ = 7.90$ MPa = 1145 psi.

This confirms the value of $\sigma_v = 7.92$ MPa reported by Ellis.[21] Thus, the ratio σ_h/σ_v in a plane perpendicular to the long axis of the tunnels is

$$\sigma_{h1}/\sigma_v = 1.17 \quad .$$

Note that this ratio is independent of the assumptions made for the rock modulus.

Finally, the virgin horizontal stress, σ_{h2} parallel to the axis of the tunnels is the normal stress on a vertical plane striking N29E. The direction cosines of the normal π_2 to this plane (Fig. 22a) would be

$$l = \cos 65^\circ = .406$$
$$m = \cos 89^\circ = .017$$
$$n = \cos 24^\circ = .913$$
$$(l^2 + m^2 + n^2 = 0.9993 \simeq 1.0) \ ,$$

so that

$$\sigma_{h2} = l^2\sigma_1 + m^2\sigma_2 + n^2\sigma_3 = 4.20 \text{ MPa} \quad .$$

With $\sigma_v = 7.90$, $\sigma_{h1} = 9.22$, and $\sigma_{h2} = 4.20$, we estimate the first invariant as

$$I_1 = 21.32 \text{ MPa} \ ,$$

which is within 0.5% of the $(\sigma_1 + \sigma_2 + \sigma_3)$ value previously calculated.

Yet another way of finding the above stresses consists of the three-dimensional Mohr constructions shown in Fig. 23. Note that they provide shear stresses as well as normal stresses on the planes of interest. The values obtained in this fashion are

$$\sigma_v = 7.90 \text{ MPa} \ , \ \sigma_{h1} = 9.25 \text{ MPa} \ , \text{ and } \sigma_{h2} = 4.20 \text{ MPa} \ .$$

The direction of the least principal horizontal stress can be inferred from Ellis' report[21] to be around N42W. This is consistent with the N45W to N50W directions reported by Zoback,[37] who based his calculations on local seismic events and direct stress measurements at and around NTS.

4.1.3 Discussion of Secondary Principal Stresses

Ellis[30] also calculated secondary principal stresses perpendicular to hole OC-2, based on the 11 readings taken. His results are summarized in Fig. 24. Several features of this figure should be noted:

- The direction of the P stress is reasonably close to vertical.
- The P stress falls between the overburden value (10.9 MPa) and the vertical stress previously calculated (7.9 MPa). For a single horseshoe-shaped tunnel in an elastic isotropic rock,[38] when $\sigma_h/\sigma_v = 1.17$, the vertical tangential stress would be (point A, Fig. 25)

$$\sigma_{tA} = 1.18 \ \sigma_v = 9.3 \text{ MPa} \ ,$$

However, with rock damage due to blasting and stress relief, the actual value should be quite lower, which it seems to be.

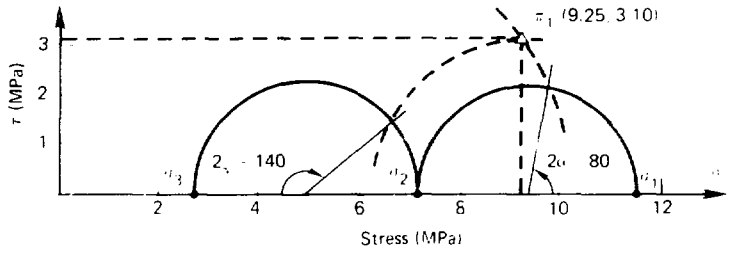

(a) Vertical plane (π_1) striking N61W

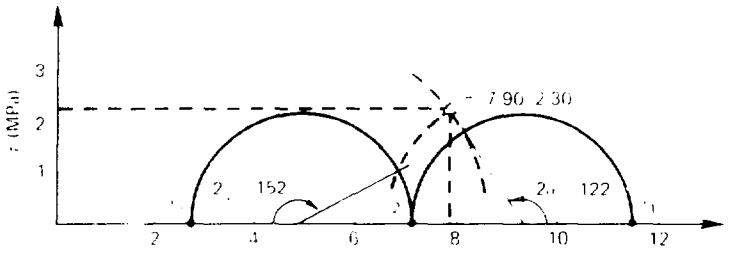

(b) Horizontal plane (π_3)

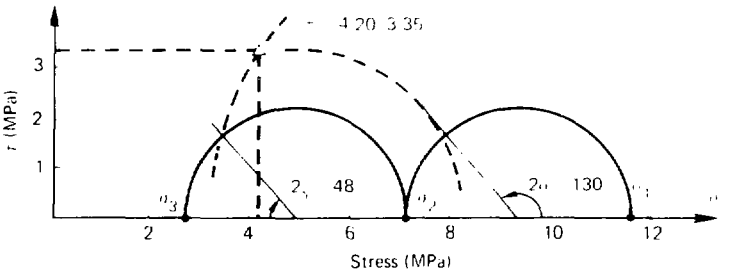

(c) Vertical plane Plane (π_2) striking N29E

FIG. 23. Three-dimensional Mohr constructions to determine normal and shear stresses on selected planes at SFT-C.

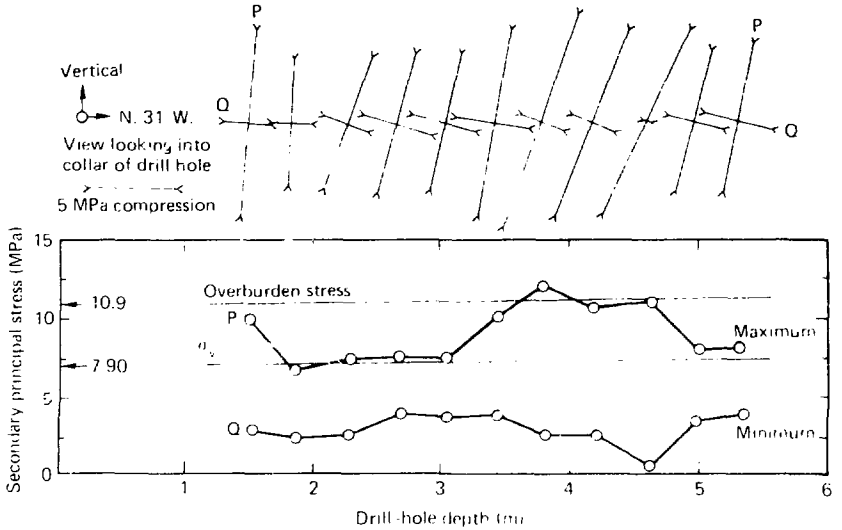

FIG. 24. Profile of secondary principal stresses at hole OC-2 (reprinted with permission from Ellis[30]).

- If we discount the first P value, the shape of the P curve is consistent with an initial zone of damaged rock followed by an arch of higher pressure. The unusual feature, however, is that the low stress zone appears to extend 3 m in from the rock face, a higher figure than would normally be expected for the depth of damaged zone around a 3.6-m wide tunnel. Typically, we would expect no more than 1 m of more fractured rock, with the higher-stress zone starting immediately behind.

- The shape of the Q curve is quite unusual because it shows significant stress reduction between 3 and 5 m, whereas the P stress has increased sharply. Numerous stress measurements in jointed rocks[22,32] usually have shown P and Q varying in the same direction.

We agree with Ellis[31] that a better picture of the stresses around SFT-C drifts should be obtained. Our own campaign of measurements was an effort in this direction.

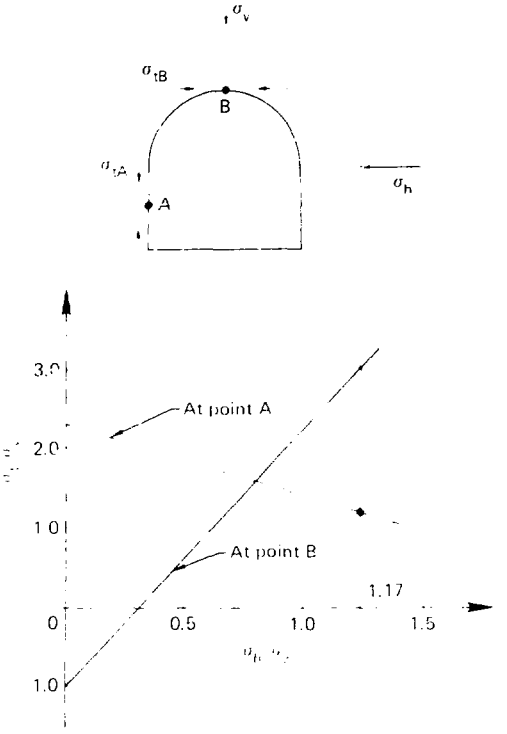

FIG. 25. Tangential stresses around a horseshoe-shaped tunnel as function of virgin stresses (reprinted with permission from Hi.amatsu and Oka[36]).

4.2 UNDERCORING STRESS MEASUREMENTS

4.2.1 Procedure and Test Results

The undercoring method can be used for near-surface measurements of tangential stresses behind a rock face.[39] Six pins are grouted in the rock--at 60° to each other--to form a rosette (Fig. 26). The rosette is then undercored by means of a central hole.

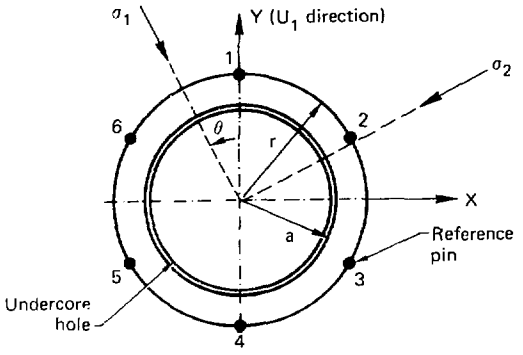

FIG. 26. Schematic of the undercoring method of stress measurement (data from Tsur-Lavie and Van Ham[39]).

The algebraic values of the three changes in diameters (U_1, U_2, U_3) between the pins are recorded. The magnitude and direction of the secondary principal stresses are calculated from

$$\sigma_1 = \frac{E}{12a}\left\{\frac{U_1 + U_2 + U_3}{M} + \frac{\sqrt{2}}{N}\left[\sum_{1,2,3}(U_i - U_j)^2\right]^{1/2}\right\},$$

$$\sigma_2 = \frac{E}{12a}\left\{\frac{U_1 + U_2 + U_3}{M} - \frac{\sqrt{2}}{N}\left[\sum_{1,2,3}(U_i - U_j)^2\right]^{1/2}\right\},$$

$$\theta = \frac{1}{2}\tan^{-1}\frac{\sqrt{3}\,(U_2 - U_3)}{2U_1 - U_2 - U_3},$$

where

$$M = \frac{(1+\nu)K}{2},\quad N = \frac{4(1-\nu^2)K - (1+\nu)K^3}{2},\quad K = \frac{a}{r},$$

and

a = radius of undercore hole, r = radius of pin rosette, E = rock modulus, ν = rock Poisson's ratio. Compression is negative.

Of the six undercorings attempted, only two were successful. Both were in the crowns of the heater drifts. In two of the unsuccessful cases, the pins were hit during the test. In the two other cases, discrete relaxation of rock joints around the rosette created displacements that could not be analyzed on the assumption of homogeneous behavior. Results from the two successful tests are shown in Fig. 27. The rock-mass modulus was taken as 14 GPa, from results of NX-borehole jack measurements in the first 30 cm of rock around the tunnels. The tangential stress perpendicular to tunnel axis is significantly larger than the longitudinal tangential stress. This is consistent with the ratio of σ_{h1} and σ_{h2}.

4.2.2 Discussion

It appears that undercoring can be a valuable substitute or complement to the use of flat-jacks. However, the procedure should be modified to enable a direct determination of the modulus at the site of the test. A possibility is to first undercore the rosette with an NX-hole in which a new version of the

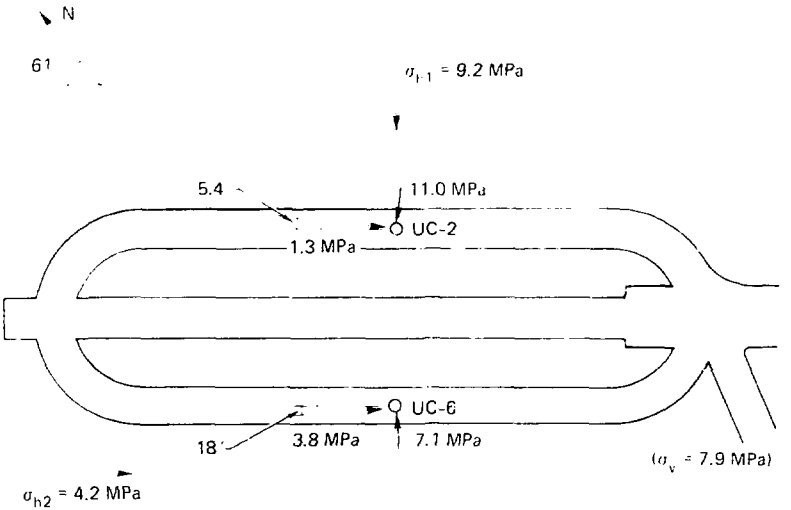

FIG. 27. Secondary principal stresses tangent to the crown of heater drifts.

borehole jack could be inserted. Then the rosette could be undercored again with a larger bit to provide redundant information.

4.3 MEASUREMENTS BY BOREHOLE JACK FRACTURING

4.3.1 The Jack-Fracturing Method

The jack-fracturing method of stress measurements was developed by De la Cruz.[40] The basic idea of this method is to strain relieve a portion of the circumference of a borehole by loading it with curved jack plates to induce radial fractures around the hole (Fig. 28).

The procedure includes the following steps:

- Friction gages are installed at a known orientation on the borehole walls.
- Loads are applied until fracture of the walls occurs, and loading is continued until the strain readings stabilize.
- Strain relief is measured as the difference between maximum strain reading and stabilized strain reading after fracture.

The strain relief, $\varepsilon_{\theta\theta}$, is a function of the normal and shear stresses away from the hole:

$$\varepsilon_{\theta\theta} = \frac{1 - \nu^2}{E} \left[(1 - 2 \cos 2\theta)\, \sigma_x + (1 + 2 \cos 2\theta)\, \sigma_y - 4 \sin 2\theta . \tau_{xy} \right] .$$

FIG. 28. Schematic of the jack-fracturing test (data from De la Cruz[40]).

Thus, if fractures are induced in at least three different orientations in the borehole (three independent operations at a sufficient distance apart), three equations such as the one above can be written. From these the field stresses σ_x, σ_y, and τ_{xy} can be obtained. The secondary principal stresses in the plane perpendicular to the axis of the borehole and their orientation can be calculated as

$$\sigma_1 = \frac{(\sigma_x + \sigma_y)}{2} + \left[\frac{(\sigma_x - \sigma_y)^2}{4} + \tau_{xy}^2 \right]^{1/2}$$

$$\sigma_2 = \frac{(\sigma_x + \sigma_y)}{2} - \left[\frac{(\sigma_x - \sigma_y)^2}{4} + \tau_{xy}^2 \right]^{1/2}$$

$$\alpha = \frac{1}{2} \tan^{-1} \frac{\tau_{xy}}{\sigma_x - \sigma_y} .$$

Using the De la Cruz convention, α is the clockwise angle between the x axis, taken vertical, and σ_1.

4.3.2 Results at SPT-C

The measurements by borehole jack fracturing were performed by De la Cruz and Voss in the four NX-holes: MBI-7 and MBI-14, north and south. Positive readings were obtained in both holes of the north pillar, but in the south pillar the degree of pre-existing fracturing apparently precluded meaningful measurements. The strains, $\varepsilon_{\theta\theta}$, are summarized in Table 7, and the calculated stresses for the north pillar are shown in Tables 8 and 9.

4.3.3 Discussion

Using the best estimate of rock-mass modulus obtained in Sec. 2, the values of σ_1 are unrealistically low while the values of σ_2 are within a range compatible with the horizontal stress values discussed in Sec. 4.1.2. The fact that the jack-fracturing method did not yield any results in the south pillar may also raise questions concerning the results obtained in the north pillar. The RQD values and the moduli measured in both pillars do not

TABLE 7. Summary of strain relief readings, jack-fracturing method.

Hole	Depth from N collar (m)	Orientation (deg. from vertical)	$\varepsilon_{\theta\theta}$ (10^{-6})
MBI-7N	1.8	45	125
	3.0	30	167
	4.2	0	312
	4.8	60	90
	5.4	45	104
MBI-14N	0.6	90	390
	1.8	30	243
	2.4	0	200
	4.2	45	300

Combining the above readings 3 by 3 (in three different orientations at the same location), the secondary principal stress values are obtained as shown in Tables 8 and 9. The rock-mass modulus is taken as 26 GPa.

tend to indicate a drastic increase in fracturing in the south pillar, which would preclude repeating the measurements of the north pillar.

Altogether, the jack-fracturing results do not appear consistent enough to be taken at face value. A re-examination of the technique is probably in order for testing in all but massive rocks. We suggest that the borehole measurements be preceded by a visual examination of the borehole wall to ascertain the presence and density of intersecting fractures. The jack could then be used in the least-fractured zones to enhance the reliability of the data.

In this research we did not attempt to measure stress changes in the vicinity of the drifts because there was not any ongoing mining or thermal loading. Hence, we did not expect stresses to vary. In any case the measurement of stress changes can be a delicate procedure. The options are to use vibrating wire stressmeters[41] or hydraulic cells.[42] Stressmeters used at SFT-C are quite rapidly attacked by corrosion. Also, the calibration of the hydraulic cells is a very complex undertaking.[41] We suggest that more

TABLE 8. Secondary principal stresses perpendicular to hole MBI-7N, north pillar.

	Orientation of combined readings (deg.)				
	0-30-45	0-30-60	0-45-60	30-45-60	Average
σ_1 (MPa)	4.32	4.27	4.78	3.97	4.33
σ_2 (MPa)	2.32	2.25	2.79	2.16	2.38
$\alpha^{(o)}$	30	29	28	27	29

TABLE 9: Secondary principal stresses perpendicular to hole MBI-14N, north pillar.

	Orientation of combined readings (deg.)				
	0-30-90	0-45-90	0-30-45	30-45-90	Average
σ_1 (MPa)	4.74	4.74	5.19	4.63	4.82
σ_2 (MPa)	3.44	3.44	3.57	3.11	3.39
$\alpha^{(o)}$	0	0	0	0	0

attention be given to the development of reliable gages to monitor stress changes over long periods of time, under unfavorable thermal and moisture conditions.

5. IN SITU POISSON'S RATIO OF CLIMAX GRANITE

If we assume the tunnels to be in a plane strain condition in their central portion where the stresses were measured, we can estimate an in situ Poisson's ratio from

$$\sigma_{h2} = \nu(\sigma_v + \sigma_{h1}) \ .$$

Here

$$\nu = 4.2/(9.2 + 7.9) = 0.246 .$$

This would seem to be a reasonable value for the Poisson's ratio of the rock mass. Note also that this value is obtained independently of any assumption made for the in situ rock-mass modulus.

6. SUMMARY AND RECOMMENDATIONS

6.1 SUMMARY

The in situ modulus of the Climax granite in the Spent Fuel Test (SFT-C) area of the Nevada Test Site was estimated using six different approaches. Our best estimate of field modulus as E_f = 26 GPa was obtained from a comparison of the various approaches. A best estimate of laboratory modulus acquired by comparing three different sources was E_l = 70 GPa. Therefore, the modulus reduction factor for the Climax granite appears to be E_f / E_l = 0.37. In turn, our estimate of in situ rock-mass deformability was used to back-calculate in situ values for the normal stiffness of the granite joints.

Our analysis of former stress measurements by the U.S. Geological Survey shows that the horizontal stresses in the vicinity of SFT-C vary greatly with azimuth. An unexplained feature of the stresses at SFT-C is the fact that the vertical stress appears to be only 65 to 75% of the calculated lithostatic burden. From the three-dimensional stress ellipsoid at mid-length in the tunnels, assuming a plane strain condition, we were able to estimate an in situ Poisson's ratio of the rock mass as ν = 0.246. Two other techniques were applied in an attempt to measure the stresses around the SFT-C heater and canister drifts: the undercoring method and the borehole jack fracturing approach. The former technique appears to have given reasonable estimates of tangential stresses in the roof of the heater drifts; the latter appears to give low results for stresses in the pillars.

Specific recommendations are made for future tests to further characterize the mechanical properties of the Climax granite and the in situ stresses at SFT-C.

6.2 RECOMMENDATIONS

- A new attempt should be made to apply the petite sismique technique at SFT-C. Additional measurements should be performed horizontally in the pillars between holes MBI-7 and MBI-14. This would possibly shed some light on the question raised by the high frequencies of shear waves measured between pillar walls.

- The NX-borehole jack (Goodman Jack) should be improved, to overcome longitudinal bending and plate contact problems. We have discussed possible design modifications with the manufacturer.

- An effort should be made to determine the normal stiffness (K_n) of granite joints in situ. This stiffness plays an important part in the modeling of both the mechanical and the hydraulic behavior of rock masses.

- The undercoring technique can be successfully reused, in a somewhat modified form, both to minimize pin contact and to obtain rock-mass modulus at the site of the stress measurements. We have conceived of a revised test procedure.

- A direct comparison should be made of flat jacks and undercoring at SFT-C. These shallow jacks should be thin half-disks emplaced in diamond-saw cut slots. The flat-jack tests can also be arranged so that they would be part of an experiment to measure normal joint stiffnesses.

- To improve the estimate of the undisturbed stress field at SFT-C, future overcoring measurements should be performed to greater depths than the previous USGS tests. This can be achieved by deepening the existing holes in the south heater drift. For correlation and technique evaluation, the mini-hydrofracturing method of the USGS should be employed in an adjacent location to the overcoring measurements. In addition, to resolve the uncertainty about the stress state in the pillars, overcoring measurements should be performed in the center section where modulus data are available.

- More reliable gages are needed to monitor stress changes over long periods of time, under unfavorable thermal and moisture conditions.

- Because of its jointing and fracturing, the stresses in the Climax pluton may not be very homogeneous. Certainly, the variability of stresses in jointed media[43] is a question that warrants further investigation.

REFERENCES

1. L. D. Ramspott, "Climax Granite Test Results," in *Proc. Workshop on Thermomech. Model. for Hardrock Waste Repository, Berkeley, Calif., 1979* (Lawrence Livermore National Laboratory, Livermore, Calif., UCAR-10043, 1979), pp. 92-112.

2. L. D. Ramspott and L. B. Ballou, "Test Storage of Spent Reactor Fuel in the Climax Granite, at the Nevada Test Site," in *Proc. Symp. Waste Management '80, Tucson, Arizona, 1980* (Lawrence Livermore National Laboratory, Livermore, Calif., UCRL-83976, 1980), 17 pp.

3. T. Schrauf and M. Board, *Instrument Selection, Installation, and Analysis of Data for the Spent Fuel Mine-bu, Nevada Test Site, Climax Stock*, Terra Tek Inc., Salt Lake City, Utah, report to Lawrence Livermore National Laboratory, TR-79-51 (1979).

4. F. E. Heuze, T. R. Butkovich, and J. C. Peterson, *An Analysis of the Mine-bu Experiment, Climax Granite, Nevada Test Site*, Lawrence Livermore National Laboratory, UCRL-85622 (1981).

5. F. E. Heuze, *JPLAXD User's Manual - A Finite Element Program for Plane and Axisummetric Analysis of Structure in Jointed Rocks, with Dilatancy*, University of Colorado, Boulder, Colo., unpublished notes (1979).

6. F. Maldonado, *Summary of the Geology and Physical Properties of the Climax Stock, Nevada Test Site*, U.S. Geological Survey, Denver, Colo., report to the Nevada Operations Office, Department of Energy (1977).

7. D. J. Wilder and W. C. Patrick, *Geotechnical Status Report for Test Storage of Spent Reactor Fuel in Climax Granite, Nevada Test Site*, Lawrence Livermore National Laboratory, Livermore, Calif., UCRL-85096 (1980).

8. R. E. Goodman, T. K. Van, and F. E. Heuze, "The Measurement of Rock Deformability in Boreholes," in *Proc. Symp. on Rock Mech., 10th, Austin, Texas, 1968* (Am. Inst. Min. Metall. Pet. Eng., New York, New York, 1972), pp. 523-555.

9. F. E. Heuze and A. Salem, "Rock Deformability Measured In Situ--Problems and Solutions," in *Proc. Int. Symp. on Field Meas. in Rock Mech., Zurich, Switzerland, 1977*, pp. 575-587.

10. W. A. Hustrulid, "An Analysis of the Goodman Jack," in *Proc. Symp. on Rock Mech., 17th, Snowbird, Utah, 1976*, pp. 4B10-1 to 4B10-8.

11. D. V. Deere, "Technical Description of Rock Cores for Engineering Purposes," *Rock Mech. and Eng. Geol.*, 1, (No. 1), 17-22 (1964).

12. R. V. De la Cruz, "Modified Borehole Jack Method for Elastic Property Determination in Rocks," *Rock Mech.*, 10, 221-289 (1978).

13. F. E. Heuze, "Scale Effects in the Determination of Rock Mass Strength and Deformability," *Rock Mech.*, 12, 167-192 (1980).

14. B. Schneider, "Moyens Nouveaux de Reconnaissance des Massifs Rocheux" (New Tools for the Exploration of Rock Masses), *Ann. Inst. Tech. Batim. Trav. Publics*, 62, 1055-1094 (1967).

15. Z. T. Bieniawski, "Determining Rock Mass Deformability: Experience from Case Histories," *Int. J. Rock Mech and Min. Sci.*, 15, (No. 5), 237-247 (1978).

16. G. B. Wallace, E. T. Slebir, and F. A. Anderson, "Foundations Testing for Auburn Dam," in *Proc. Symp. on Rock Mech., 11th, Berkeley, Calif., 1969* (Am. Inst. Min. Metall. Pet. Eng., New York, New York, 1970), pp. 461-498.

17. Z. T. Bieniawski, "The Geomechanics Classification in Rock Engineering Applications," in *Proc. Congr. Int. Soc. Rock Mech., 4th, Montreux, Switzerland, 1979*, vol. 2, pp. 41-48.

18. N. Barton, R. Lien, and J. Lunde, "Application of Q-System in Design Decisions Concerning Dimensions and Appropriate Support for Underground Installations," *Proc. Rockstore '80 Symp. Stockholm, Sweden, 1980* (Pergamon Press Inc. Elmsford, N.Y., 1980), vol. 2, pp. 553-561.

19. G. E. Wickham and H. R. Tiedemann, *Ground Support Prediction Model (RSR Concept)*, Jacobs Associates, San Francisco, Calif., report to U.S. Bureau of Mines on ARPA Contract H0220075, AD-773018 (1974).

20. H. R. Pratt, R. Lingle, and T. Schrauf, *Laboratory Measured Material Properties of Quartz Monzonite, Climax Stock, Nevada Test Site*, Terra Tek, Inc., Salt Lake City, Utah, report to Lawrence Livermore National Laboratory, UCRL-15073 (1979).

21. W. L. Ellis, U.S. Geological Survey, Denver, Colo., private communication to L. D. Ramspott, Lawrence Livermore National Laboratory (June 7, 1979).

22. F. E. Heuze, *The Design of Room-and-Pillar Structures in Competent Jointed Rock. Example: The Crestmore Mine, California*, Doctor of Engineering Dissertation, University of California, Berkeley, Calif. (1970).

23. F. E. Heuze, "Sources of Errors in Rock Mechanics Field Measurements and Related Solutions," *Int. J. Rock Mech. and Min. Sci.*, 8, (No. 4), 297-310 (1971).

24. S. D. Priest and J. A. Hudson, "Discontinuity Spacings in Rock," *Int. J. Rock Mech. and Min. Sci.*, 13, 135-148 (1976).

25. P. F. Wallis and M. S. King, "Discontinuity Spacings in a Crystalline Rock," *Int. J. Rock Mech. and Min. Sci.*, 17, 63-66 (1980).

26. N. Barton and S. Bandis, "Some Effects of Scale on the Shear Strength of Joints," *Int. J. Rock Mech. and Min. Sci.*, 17, 69-73 (1980).

27. R. E. Goodman, *Methods of Geological Engineering*, (West Publishing Co., St. Paul, Minn., 1976), 472 pp.

28. F. E. Heuze, R. E. Goodman, and A. Bornstein, "Joint Perturbation and No-Tension Finite Element Solutions," *Rock Mech.*, 3, 13-24 (1971).

29. P. A. Witherspoon, J. S. Wang, K. Iwai, and J. E. Gale, *Validity of Cubic Law for Fluid Flow in a Deformable Fracture*, Lawrence Berkeley Laboratory, Berkeley, Calif., LBL-9557 (1979).

30. W. L. Ellis, U.S. Geological Survey, Denver, Colo., private communication to L. D. Ramspott, Lawrence Livermore National Laboratory, Livermore, Calif. (June 22, 1979).

31. W. L. Ellis, U.S. Geological Survey, Denver, Colo., private communication to R. C. Carlson, Lawrence Livermore National Laboratory, Livermore, Calif. (June 13, 1980).

32. R. H. Merrill, *Three-Component Borehole Deformation Gage for Determining the Stress in Rock*, U.S. Bureau of Mines, Washington, D.C., RI-7015 (1967).

33. G. E. Brethauer and J. G. Rosenbaum, *Calculation of In Situ Principal Stress Using Secondary Principal Stress*, U.S. Geological Survey, Denver, Colo., report to Defense Nuclear Agency, 474-181 (1975).

34. Y. Hiramatsu and Y. Oka, "Determination of the Stress in Rock Unaffected by Boreholes and Drifts, from Measured Strains or Deformations," *Int. J. Rock Mech. Mining Sci.*, 5, 337-353 (1968).

35. L. Panek, *Calculation of the Average Stress or Strain from Measurement of the Diametral Deformation of a Drill Hole*, U.S. Bureau of Mines, Washington, D.C., RI-6732 (1960). (Also in Special Technical Publication Am. Soc. Test. Mat. STP-402, Philadelphia, Pa., 1966.)

36. R. E. Goodman, "The Resolution of Stresses in Rock Using Stereographic Projection," *Int. J. Rock Mech. and Min. Sci.*, 1, 93-103 (1964).

37. M. L. Zoback and M. Zoback, "State of Stress in the Coterminous United States," *J. Geophys Res.*, 85 (No. 311), 6113-6156 (1980).

38. Y. Hiramatsu and Y. Oka, "Stress on the Wall Surface of Levels with Cross Sections of Various Shape," *Int. J. Rock Mech. and Min. Sci.*, 1, 199-216 (1964).

39. Y. Tsur-Lavie and F. Van Ham, "Accuracy of Strain Measurements by the Undercoring Method," in *Proc. Congress Int. Soc. for Rock Mech., 3rd, Denver, Colo., 1974*, vol. II-A, pp. 474-480.

40. R. V. De la Cruz, "Jack Fracturing Technique of Stress Measurements," *Rock Mech.* 9, 27-42 (1977).

41. P. K. Dutta, R. W. Hatfield, and P. . Runstadler, Jr., *Room and High Temperature Calibration Characteristics of IRAD Gage Vibrating Wire Stressmeter*, IRAD Gage Co., Lebanon, N. H., report to Lawrence Livermore National Laboratory, Tech. Report 80-2 (1980).

42. C. H. Miller, J. D. Kibler, and J. R. Eye, *A New, Permanent-Installation Device for Monitoring Stress Changes in NX Core-Holes*, U.S. Geological Survey, Denver, Colo., report to Defense Nuclear Agency, 474-214 (1975).

43. B. Singh, "Continuum Characterization of Jointed Rock Masses. Part I: The Constitutive Equations. Part II: Signficance of Low Shear Modulus," *Int. J. Rock Mech. and Min. Sci.*, 10, 311-349 (1973).

CG/ga

U. S. Government Printing Office 1981/4 789-002/5562